Reply to editor corrections (R2)

Comment Figure 1: your study site is indicated with a red asterisk. It isn't easily distinguished on the figure in its current size, and there is a danger that the asterisk will be very difficult to identify if the figure is reduced in size during proofing. Is it possible for you to make this symbol larger / more bold / outlined in black so that it isn't lost in the graphic?
Reply: we have changed the figure and inserted a larger asterisk outlined in black in Figure 1

Comment - line 515: write "excluding" in full rather than "excl"
Reply: corrections made

Comment - Figure 3: can you clarify in the caption what the red line is on the T/M ratio? I'm assuming some smoothing function but i couldn't find an explanation in the text or supplemental figures.
Reply: explanation added in caption fig3, line is a LOWESS smoother

Comment - lines 581-583: can you clarify the time frame of this delta front advance, since it is not clear from this text nor from the figure caption (are you talking about patterns of change restricted to the same time interval covered by your record, or something longer term?)
Reply: we added the age range for the main advance in the main text (discussion) and in the figure caption of Supl. Figure 1

Comment - lines 584-585: sentence starting "In- or exclusion..". I would recommend trying to edit this sentence as it is a bit confusing. Perhaps "Bisaccate pollen is the component most sensitive to differential transport processes, yet regardless of whether it is included in the T/M index (Fig. S5) the same patterns are recorded, indicating no direct influence of differential transport on the T/M ratio" ?
Reply: we adopted the suggestion of the editor

Comment - throughout the manuscript there are some incidents of "G-IC cycle" being used, but I assume this should be "G-IG cycle" if you are discussing glacial-interglacial cycles?
Reply: Use of G-IC corrected

Comment - supplemental figure S3: can you clarify in the caption which of these tie points is from which method e.g. are those with the large age uncertainties the biostratigraphy tie points? Were all tie points used (Table S1 seems to suggest some big discrepancies between e.g. dinocyst datums and the others which are listed). Different colours / shading for different methods might help on the graphic.
Reply: we have adapted supl Figure 2 indicating the type of age tie point. The figure does not contain the Miocene ages from Table S1 as they are prior to a hiatus, which has now been explained in the caption. The only other point omitted form the figure is described as very scattered in the table, and hence not useable.

Comment - Table S1 (chronostratigraphic tie points): can you clarify in the caption whether the first 'age'

column is the age that you have assigned to that particular depth in A15-3? (and then the min/max age as being those assigned to the datum in the literature?).

Reply: we have changed the header and information in the table caption, range indicates indeed the min and max from recent literature.

Land-sea coupling of early Pleistocene glacial cycles in the southern North Sea exhibit dominant Northern Hemisphere forcing

Timme H. Donders[1,2], Niels A.G.M. van Helmond[3], Roel Verreussel[2], Dirk Munsterman[4], Johan Ten Veen[4], Robert P. Speijer[5], Johan W.H. Weijers[3]*, Francesca Sangiorgi[3], Francien Peterse[3], Gert-Jan Reichart[3,6], Jaap S. Sinninghe Damsté[3,6], Lucas Lourens[3], Gesa Kuhlmann[7] and Henk Brinkhuis[3,6]

[1] Department of Physical Geography, Fac. of Geosciences, Utrecht University, Heidelberglaan 2, 3584CD, Utrecht, The Netherlands.

[2] TNO - Applied Geosciences, Netherlands Organisation of Applied Scientific Research Princetonlaan 6, 3584 CB Utrecht, The Netherlands.

[3] Department of Earth Sciences, Fac. of Geosciences, Utrecht University, Heidelberglaan 2, 3584CS, Utrecht, The Netherlands.

[4] TNO - Geological Survey of the Netherlands, Netherlands Organisation of Applied Scientific Research, Princetonlaan 6, 3584 CB Utrecht, The Netherlands.

[5] Department of Earth and Environmental Sciences, KU Leuven, 3001 Heverlee, Belgium

[6] NIOZ Royal Netherlands Institute for Sea Research, P.O. Box 59, 1790 AB, Den Burg, Texel, The Netherlands

[7] BGR - Federal Institute for Geosciences and Natural Resources, Geozentrum Hannover Stilleweg 2, D-30655 Hannover

* Currently at: Shell Global Solutions International B.V., Grasweg 31, 1031 HW, Amsterdam, The Netherlands

Correspondence to: t.h.donders@uu.nl

Abstract

We assess the disputed phase relations between forcing and climatic response in the early Pleistocene with a spliced Gelasian (~2.6 – 1.8 Ma) multi-proxy record from the southern North Sea basin. The cored sections couple climate evolution on both land and sea during the intensification of Northern Hemisphere Glaciations (NHG) in NW Europe, providing the first well-constrained stratigraphic sequence of the classic terrestrial Praetiglian Stage. Terrestrial signals were derived from the Eridanos paleoriver, a major fluvial system that contributed a large amount of freshwater to the northeast Atlantic. Due to its latitudinal position, the Eridanos catchment was likely affected by early Pleistocene NHG, leading to intermittent shutdown and reactivation of river flow and sediment transport. Here we apply organic geochemistry, palynology, carbonate isotope geochemistry, and seismostratigraphy to document both vegetation changes in the Eridanos catchment and regional surface water conditions and relate them to early Pleistocene glacial-interglacial cycles and relative sea-level changes. Paleomagnetic and palynological data provide a solid integrated timeframe that ties the obliquity cycles, expressed in the borehole geophysical logs, to Marine Isotope Stages (MIS) 103 to 92, independently confirmed by a local benthic oxygen isotope record. Marine and terrestrial palynological and organic geochemical records provide high resolution reconstructions of relative Terrestrial and Sea Surface Temperature (TT and SST), vegetation, relative sea level, and coastal influence.

During the prominent cold stages MIS 98 and 96, as well as MIS 94 the record indicates increased non-arboreal vegetation, and low SST and TT, and low relative sea level. During the warm stages MIS 99, 97 and 95 we infer increased stratification of the water column together with higher % arboreal vegetation, high SST and relative sea-level maxima. The early Pleistocene distinct warm-cold alterations are synchronous between land and sea, but lead the relative sea-level change by 3-8 thousand years. The record provides evidence for a

dominantly NH driven cooling that leads the glacial build up and varies on obliquity timescale. Southward migration of Arctic surface water masses during glacials, indicated by cool-water dinoflagellate cyst assemblages, is furthermore relevant for the discussion on the relation between the intensity of the Atlantic meridional overturning circulation and ice sheet growth.

Keywords: Glacial-interglacial climate, palynology; organic geochemistry; obliquity, land-sea correlation, Eridanos delta, southern North Sea

1 Introduction

The build-up of extensive Northern Hemisphere (NH) land ice started around 3.6 Ma ago (Ruddiman et al. 1986; Mudelsee and Raymo, 2005; Ravelo et al., 2004; Ravelo, 2010), with stepwise intensifications between 2.7 and 2.54 Ma ago (e.g., Shackleton and Hall, 1984; Raymo et al., 1989; Haug et al., 2005; Lisiecki and Raymo, 2005; Sosdian and Rosenthal, 2009). In the North Atlantic region the first large-scale early Pleistocene glaciations, Marine Isotope Stages (MISs) 100 - 96, are marked by e.g. appearance of ice-rafted debris and southward shift of the Arctic front (see overviews in Naafs et al., 2013; Hennissen et al., 2015). On land, the glaciations led to faunal turnover (e.g. Lister, 2004; Meloro et al., 2008) and widespread vegetation changes (e.g. Zagwijn, 1992; Hooghiemstra and Ran, 1994; Svenning, 2003; Brigham-Grette et al., 2013). Many hypotheses have been put forward to explain the initiation of these NH glaciations around the Plio-Pleistocene transition interval. Causes include tectonics (Keigwin, 1982, Raymo, 1994; Haug and Tiedemann, 1998; Knies et al, 2004; Poore et al., 2006), orbital forcing dominated by obliquity-paced variability (Hays et al., 1976; Maslin et al., 1998; Raymo et al., 2006) and atmospheric CO_2 concentration decline (Pagani et al., 2010; Seki et al., 2010; Bartoli et al., 2011) driven by e.g. changes in ocean stratification that affected the biological pump (Haug et al., 1999). Changes were amplified by NH albedo changes (Lawrence et al., 2010), evaporation feedbacks (Haug et al., 2005), and possibly tropical atmospheric circulation change and breakdown of a permanent El Niño (Ravelo et al., 2004; Brierley and Fedorov, 2010; Etourneau et al., 2010).

Key aspects in this discussion are the phase relations between temperature change on land, in the surface and deep ocean, and ice sheet accretion (expressed through global eustatic sea-level lowering) in both Northern and Southern Hemispheres. According to Raymo et al.

(2006), early Pleistocene obliquity forcing dominated global sea level and $\delta^{18}O_{benthic}$, because precession-paced changes in the Greenland and Antarctic ice sheets cancelled each other out. In this view, climate records independent of sea-level variations should display significant variations on precession timescale. Recent tests of this hypothesis indicate that early Pleistocene precession signals are prominent in both Laurentide ice sheet meltwater pulses and iceberg-rafted debris of the East Antarctic ice sheet, and decoupled from marine $\delta^{18}O$ (Patterson et al., 2014; Shakun et al., 2016). Alternatively, variations in the total integrated summer energy, which is obliquity controlled, might be responsible for the dominant obliquity pacing of the early Pleistocene (Huybers, 2011; Tzedakis et al., 2017). The dominance of the obliquity component has been attributed to feedbacks between high-latitude insolation, albedo (sea-ice and vegetation) and ocean heat flux (Koenig et al., 2011; Tabor et al., 2014). Sosdian and Rosenthal (2009) suggested that temperature variations, based on benthic foraminifer magnesium/calcium (Mg/Ca) ratios from the North Atlantic, explain a substantial portion of the global variation in the $\delta^{18}O_{benthic}$ signal. Early Pleistocene North Atlantic climate responses were closely phased with $\delta^{18}O_{benthic}$ changes, evidenced by dominant 41-kyr variability in North American biomarker dust fluxes at IODP Site U1313 (Naafs et al., 2012), suggesting a strong common NH high latitude imprint on North Atlantic climate signals (Lawrence et al., 2010). Following this reasoning, glacial build-up should be in phase with decreases in NH sea surface temperatures (SST) and terrestrial temperatures (TT).

To explicitly test this hypothesis we perform a high-resolution multiproxy terrestrial and marine palynological, organic geochemical, and stable isotope study on a marginal marine sediment sequence from the southern North Sea (SNS) during the early Pleistocene “41 kyr-world”. We investigate the leads and lags of regional marine vs. terrestrial climatic cooling

during MIS 102-92, and assess the local sea-level response relative to global patterns from the $\delta^{18}O_{benthic}$ stack of Lisiecki and Raymo (2005; LR04). In a dominantly, NH obliquity driven scenario, we expect the marine and terrestrial temperature proxies to be in phase on obliquity timescales with a short (less than 10 kyr) lead on sea-level variations. In addition, the record can better constrain the signature and timing of the regional continental Praetiglian stage (Van der Vlerk and Florschütz, 1953; Zagwijn, 1960) that is still widely used, although its stratigraphic position and original description are not well defined (Donders et al., 2007; Kemna and Westerhoff, 2007).

2 Geological setting

During the Neogene the epicontinental North Sea Basin was confined by landmasses except towards the northwest, where it opened into the Atlantic domain (Fig. 1) (Bijlsma, 1981; Ziegler, 1990). Water depths in the central part were approximately between 100 to 300 m as deduced from seismic geometry (Huuse et al., 2001; Overeem et al., 2001). In contrast, the recent North Sea has an average depth between 20-50 m in the south that deepens only towards the shelf edge towards 200 m in the north-west (e.g., Caston, 1979). From the present-day Baltic region a formidable river system, known as the Eridanos paleoriver, developed which built up the Southern North Sea delta across southern Scandinavia (Sørensen et al., 1997; Michelsen et al., 1998; Huuse et al., 2001; Overeem et al., 2001).

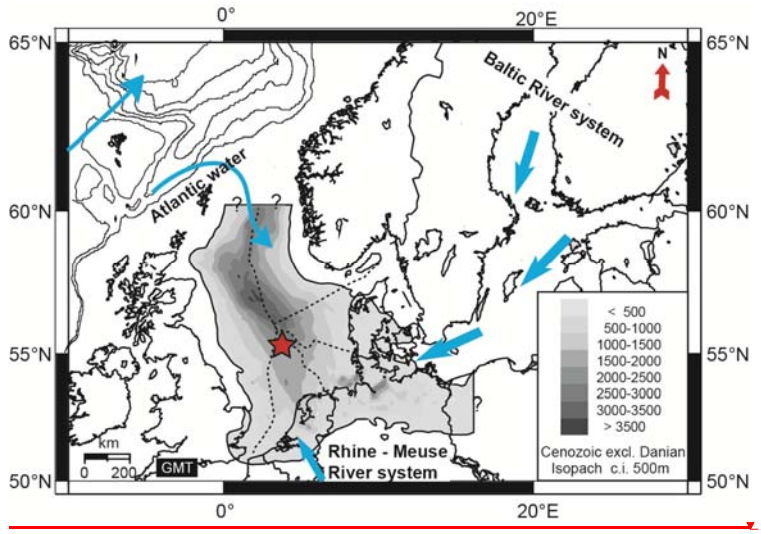

Deleted: <object>

Figure 1: Geographical map of the present day North Sea region with the superimposed thickness of Cenozoic sediment infill after Ziegler (1990) and the offshore sectors (dashed lines). The reconstructed different water sources (see Gibbard and Lewin, 2016) that influenced the Pliocene and early Pleistocene North Sea hydrography ,including the freshwater supply of the Baltic river system, the Rhine-Meuse river system and Atlantic surface waters are indicated with blue arrows. The location of both boreholes A15-3 (UTM X 552567.1, Y 6128751.6) and A15-4 (UTM X 557894.4, Y 6117753.5) is marked by an asterisk, see Fig. S1 for details.

This delta was characterized by an extensive distributary system that supplied large amounts of freshwater and sediment to the shelf sea during the Neogene and early Pleistocene (Overeem et al., 2001), resulting in a sediment infill of ~1500 m in the central North Sea Basin (Fig. 1). This system was fed by rainfall as well as by melt-water originating from Scandinavian glaciers (Kuhlmann et al., 2004), principally from the Baltic Shield in the east with some contribution from the south (Fig. 1) (Bijlsma, 1981; Kuhlmann, 2004). The

sedimentation rates reached up to 84 cm/kyr at the studied locations (Fig. 2) (Kuhlmann et al., 2006b). Today, the continental river runoff contributes only 0.5 % of the water budget in the North Sea (Zöllmer and Irion, 1996) resulting in sedimentation rates ranging between 0.4 to 1.9 cm/kyr in the Norwegian Channel, and 0.5 - 1 cm/kyr in the southern part of the North Sea (de Haas et al., 1997).

3 Material, core description and age model

Recent exploration efforts in the SNS led to the successful recovery of cored sedimentary successions of marine isotope stages (MIS) 102-92 and continuous paleomagnetic logs (Fig. 2) (Kuhlman et al, 2006ab). For quantitative palynological and geochemical analyses, discrete sediment samples were taken from two exploration wells A15-3 and A15-4 located in the northernmost part of the Dutch offshore sector in the SNS at the Neogene sedimentary depocentre (Fig. 1). An integrated age model is available based on a multidisciplinary geochronological analysis of several boreholes within the SNS (Kuhlmann et al., 2006a,b) and dinocyst biostratigraphy. The magnetostratigraphy, core correlation and age-diagnostic dinocyst events used for this age-model are summarized in Fig. 2 and Table S1. The recovered material mainly consists of fine-grained, soft sediments (clayey to very fine sandy), sampled from cuttings, undisturbed sidewall cores and core sections (Fig. 2). Geochemical analyses were limited to the (sidewall) core intervals, while the cuttings were to increase resolution of the palynological samples, and are based on larger rock chips that have been cleaned before treatment. Clear cyclic variations in the gamma ray signal and associated seismic reflectors across the interval can be correlated across the entire basin (Kuhlman et al., 2006a; Kuhlmann and Wong, 2008; Thöle et al. 2014). Samples from the two boreholes were spliced based on the gamma-ray logs (Figs. 2, S2) and biostratigraphic events to generate a composite record. The age model is mainly based on continuous paleomagnetic logging

supported by discrete sample measurements and high-resolution biostratigraphy. There is evidence of small hiatuses above (~2.1 Ma) and significant hiatuses below the selected interval (within the early Pliocene and Miocene, particularly the Mid-Miocene Unconformity), which is why we excluded these intervals in this study. The position of the Gauss-Matuyama transition at the base of log unit 6 correlates to the base of MIS 103, the identification of the X-event, at the top of log unit 9, correlates to MIS 96, and the Olduvai magnetochron is present within log units 16-18 (Kuhlmann et al., 2006a,b). These ages are supported by dinocyst and several other bioevents (Table S1, updated from Kuhlmann et al., 2006a,b). Consistent with the position of the X-event, the depositional model by Kuhlmann and Wong (2008) relates the relatively coarse-grained, low gamma ray intervals to interglacials characterized by high run off. A recent independent study on high-resolution stable isotope analyses of benthic foraminifera from an onshore section in the same basin confirmed this phase relation (Noorbergen et al., 2015). Around glacial terminations, when sea level was lower but the basin remained fully marine, massive amounts of very fine-grained clayey to fine silty material were deposited in the basin, the waste-products of intense glacial erosion. During interglacials with high sea level more mixed, coarser-grained sediments characterize the deposits, also reflecting a dramatically changed hinterland, retreated glaciers, and possibly (stronger) bottom currents (Kuhlmann and Wong, 2008). Based on this phase relation, detailed magneto- and biostratigraphy, grain size measurements, and previous low resolution relative SST indices (Kuhlmann et al., 2004; Kuhlmann et al., 2006a,b), the finer grained units are consistently correlated to MIS 102 – 92. Based on this correlation of the GR inflection points to the corresponding LR04 MIS transitions, the sequence is here transferred to an age scale through interpolation with a smoothing spline function (Fig. S3).

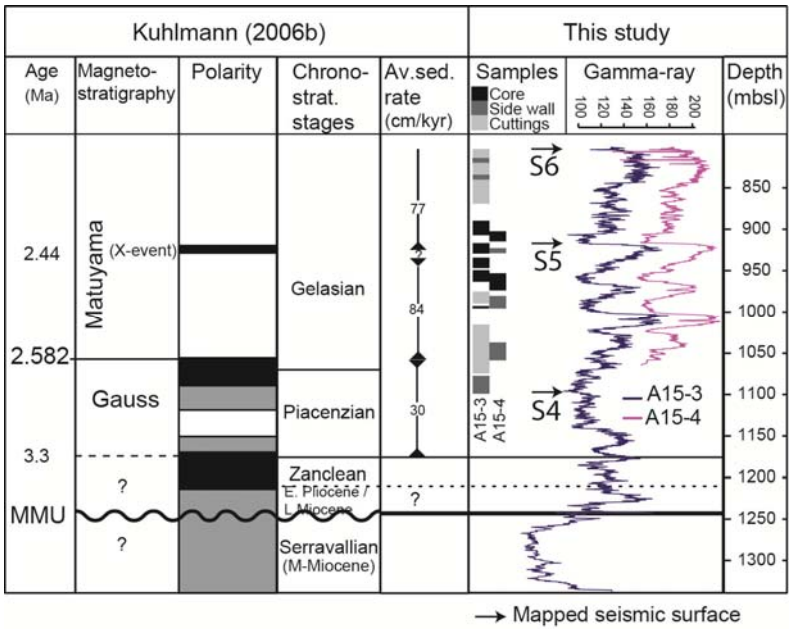

Figure 2: Chronology and mean sedimentation rates as derived from biostratigraphy and paleomagnetic data (Kuhlmann et al., 2006a,b) in combination with the gamma-ray log of A15-3 and A15-4 used in this study on a common depth scale. The position of various sample types and the mapped seismic horizons S4-6 (Fig. S1) are indicated. Material for the sidewall cores is limited, and used only for palynology and organic geochemistry. Bioevents based on Kuhlmann et al. (2006a,b) are listed in Table S1.

The regional structure and development of the delta front across the Plio-Pleistocene transition interval is very well constrained by a high-resolution regional geological model that represents the anatomy of the Eridanos (pro-) delta (Kuhlmann and Wong, 2008; Ten Veen et al., 2013). A total of 25 seismic horizons in the Plio-Pleistocene transition interval were mapped using series of publically available 2D and 3D seismic surveys across the northern part of the Dutch offshore sector. For all these surfaces the distribution of delta elements such as of topset-, foreset- and toeset-to-prodelta has been determined, resulting in zonal maps (250 m grid size) that represent the present day geometry of the surfaces. The

paleoenvironmental reconstructions are compared to these maps to constrain the regional setting and aid the interpretations.

4 Paleoenvironmental proxies and methods

4.1 Benthic oxygen and carbon isotopes ($\delta^{18}O_b$ and $\delta^{13}C_b$)

Oxygen and carbon isotopes were measured on tests of *Cassidulina teretis*, a cold water species of endobenthic foraminifera that is generally abundant in the samples and common in fine-grained sediment and relatively low salinities (Mackensen and Hald, 1988; Rosoff and Corliss, 1992). Because of their endobenthic habitat, they record isotope compositions of pore waters, which leads to somewhat reduced ($\delta^{13}C_b$) values compared to the overlying bottom waters. Since the amount of material from the sidewall cores is limited, the isotope data is only produced for the cored intervals with the principal aim to confirm the phase relationship described by Kuhlmann and Wong (2008) between facies and climate. Preservation was based on a visual inspection and assignment of a relative preservation scale of 1-5, after which the poorest 2 classes were discarded because primary calcite was nearly absent. The best preserved specimens (cat. 1) had shiny tests (original wall calcite) and showed no signs of overgrowth. Category 2 specimens showed signs of overgrowth but were not recrystallized and cat. 3 specimens were dull and overgrown by a thin layer of secondary calcite. Between ~20 and 50 µg of specimens per sample was weighed after which the isotopes of the carbonate were measured using a Kiel III device coupled to a 253 ThermoFinnigan MAT instrument. Isotope measurements were normalized to an external standard 'NBS-19' ($\delta^{18}O$ = -2.20‰, $\delta^{13}C$ = 1.95‰)..

4.2 Palynological proxies

In modern oceans, dinoflagellates are an important component of the (phyto-)plankton. About 15-20% of the marine dinoflagellates form an organic walled cyst (dinocyst) during the life cycle that can be preserved in sediments (Head, 1996). Dinocyst distribution in marine surface sediments has shown to reflect changes in the sea surface water properties, mostly responding to temperature (e.g., Rochon et al., 1999; Zonneveld et al., 2013). Down-core changes in dinocyst assemblages are widely used in reconstructing past environmental changes in the Quaternary (e.g., de Vernal et al., 2009), but also in the Neogene and Paleogene (e.g., Versteegh and Zonneveld, 1994; Head et al., 2004; Pross and Brinkhuis, 2005; Sluijs et al., 2005; Schreck et al., 2013; De Schepper et al., 2011; 2013; Hennissen et al., 2017).

Here we use the preference of certain taxa to cold-temperate to arctic surface waters to derive sea surface temperature (SST) trends. The cumulative percentage of the dinocysts *Filisphaera microornata, Filisphaera filifera, Filisphaera sp., Habibacysta tectata and B. tepikiense* on the total dinocysts represents our cold surface water indicator (Versteegh and Zonneveld, 1994; Donders et al., 2009; De Schepper et al., 2011). Interestingly, *Bitectatodinium tepikiense*, the only extant dinocyst among our cold-water species, has been recorded from the mixing zone of polar front oceanic waters with cold brackish meltwaters from glacier ice (e.g., Bakken and Dale, 1986) and at the transition between the subpolar and temperate zones (Dale, 1996). The combined abundance of *Lingulodinium machaerophorum, Tuberculodinium vancampoae*, *Polysphaeridium zoharyi* and *Operculodinium israelianum* is used here to indicate, coastal waters, although they generally also relate to warmer conditions. In particular, high percentages of *L. machaerophorum* are typically recorded in eutrophic coastal areas where reduced salinity and (seasonal) stratification due to runoff occur (Dale, 1996; Sangiorgi and Donders, 2004; Zonneveld et al., 2009). At present, *T. vancampoae*, *P.*

zoharyi and *O. israelianum* are also found in lagoonal euryhaline environments (Zonneveld et al., 2013), and hence could be used to indicate a more proximal condition relative to *L. machaerophorum* (Pross and Brinkhuis, 2005).

At present, Protoperidinioid (P) cysts are mostly formed by heterotrophic dinoflagellates and the percentage of P-cysts may be used as indicator of high eukaryotic productivity (cf. Reichart and Brinkhuis, 2003; Sangiorgi and Donders, 2004; Sluijs et al., 2005). Here we use the percentage of P-cysts (*Brigantedinium* spp., *Lejeunecysta* spp., *Trinovantedinium glorianum*, *Selenopemphix* spp., *Islandinium* spp., *Barssidinium graminosum*, and *B. wrennii*) to indicate eukaryotic productivity.

Terrestrial palynomorphs (sporomorphs) reflect variations in the vegetation on the surrounding land masses and provide information on climate variables such as continental temperatures and precipitation (e.g. Heusser and Shackleton, 1979; Donders et al., 2009; Kotthoff et al., 2014). A ratio of terrestrial to marine palynomorphs (T/M ratio) is widely used as a relative measure of distance to the coast and thereby reflects sea-level variations and depth trends in the basin (e.g. McCarthy and Mudie, 1998; Donders et al., 2009; Quaijtaal et al., 2014; Kotthoff et al., 2014). Morphological characteristics of late Neogene pollen types can, in most cases, be related to extant genera and families (Donders et al., 2009; Larsson et al., 2011; Kotthoff et al., 2014). In A15-3/4, the relatively long distance between the land and the site of deposition means that the pollen assemblage is not only a reflection of vegetation cover and climate, but includes information on the mode of transport. Assemblages with a relatively high number of taxa, including insect pollinated forms, are indicative of substantial pollen input through water transport (Whitehead, 1983), whereas wind-transported pollen typically show a low-diversity. Sediments of a location proximal to a river delta likely receive

284 a majority of pollen that is water-transported, while distal locations are dominated by wind-
285 transported pollen and particularly bisaccate taxa (Hooghiemstra, 1988; Mudie and McCarthy,
286 1994). To exclude these effects, the percentage of arboreal pollen (AP), representing relative
287 terrestrial temperatures, was calculated excluding bisaccate forms. The non-arboreal pollen
288 (NAP; mainly Poaceae and also *Artemisia*, Chenopodiaceae and Asteraceae) consist only of
289 non-aquatic herbs. High AP percentages indicate warm, moist conditions, whereas open
290 vegetation (NAP and Ericaceae) is indicative for cooler, drier conditions consistent with a
291 glacial climate (Faegri et al, 1989).
292
293 *4.3 Palynological processing*
294 The samples were processed using standard palynological procedures (e.g., Faegri et al.,
295 1989) involving HCl (30%) and cold HF (40%) digestion of carbonates and silicates.
296 Residues were sieved with 15 μm mesh and treated by heavy liquid separation (ZnCl, specific
297 gravity 2.1 g/cm^3). The slides were counted for dinocysts (with a minimum of 100 cysts) and
298 pollen (with a preferable minimum of 200 grains). The dinocyst taxonomy follows Williams
299 et al. (2017). Resulting counts were expressed as percent abundance of the respective
300 terrestrial or marine groups of palynomorphs.
301
302 *4.4 Organic geochemical proxies*
303 We applied three measures for the relative marine versus terrestrial hydrocarbon
304 sources. The Carbon Preference Index (CPI), based on C_{25}-C_{34} *n*-alkanes, originally devised to
305 infer thermal maturity (Bray and Evans, 1961), has high values for predominantly terrestrial
306 plant sources (Eglinton and Hamilton, 1967; Rieley et al., 1991). Values closer to one indicate
307 greater input from marine microorganisms and/or recycled organic matter (e.g., Kennicutt et
308 al., 1987). Furthermore, peat mosses like *Sphagnum* are characterized by a dominance of the

309 shorter C_{23} and C_{25} n-alkanes (e.g. Baas et al., 2000; Vonk and Gustafsson, 2009), whereas
310 longer chain n-alkanes (C_{27}-C_{33}) are synthesized by higher plants (e.g., Pancost et al., 2002;
311 Nichols et al., 2006) . Here we express the abundance of *Sphagnum* relative to higher plants
312 as the proportion of C_{23} and C_{25} relative to the C_{27}-C_{33} odd-carbon-numbered n-alkanes.
313 Finally, the input of soil organic matter into the marine environment was estimated using the
314 relative abundance of branched glycerol dialkyl glycerol tetraethers (brGDGTs), produced by
315 bacteria that are abundant in soils, versus that of the marine Thaumarchaeota-derived
316 isoprenoid GDGT crenarchaeol (Sinninghe Damsté et al., 2002), which is quantified in the
317 Branched and Isoprenoid Tetraether (BIT) index (Hopmans et al., 2004). The distribution of
318 brGDGTs in soils is temperature dependent (Weijers et al., 2007; Peterse et al., 2012). Annual
319 mean air temperatures (MAT) were reconstructed based on down-core distributional changes
320 of brGDGT and a global soil calibration that uses both the 5- and 6-methyl isomers of the
321 brGDGTs (MAT_{mr}; De Jonge et al., 2014a). Cyclisation of Branched Tetraethers (CBT)
322 ratios, was shown earlier to correlate with the ambient MAT and soil pH (Weijers et al., 2007;
323 Peterse et al., 2012). The much improved CBT' ratio (De Jonge et al., 2014a), which includes
324 the pH dependent 6-methyl brGDGTs, is used here to reconstruct soil pH. The Total Organic
325 Carbon (TOC) and total nitrogen measurements are used to determine the atomic C/N ratio
326 that in coastal marine sediments can indicate the dominant source of organic matter, with
327 marine C/N values at ~10 and terrestrial between 15 and 30 (Hedges et al., 1997).
328
329 *4.5 Organic geochemical processing*
330 Organic geochemical analyses were limited to the core and sidewall core samples. For
331 TOC determination ~ 0.3 g of freeze dried and powdered sediment was weighed, and treated
332 with 7.5 ml 1 M HCL to remove carbonates, followed by 4 h shaking, centrifugation and
333 decanting. This procedure was repeated with 12 h shaking. Residues were washed twice with

demineralised water dried at 40-50°C for 96 h after which weight loss was determined. ~15 to 20 mg ground sample was measured in a Fisons NA1500 NCS elemental analyzer with a normal Dumas combustion setup. Results were normalized to three external standards (BCR, atropine and acetanilide) analyzed before and after the series, and after each ten measurements. % TOC was determined by %C x decalcified weight/original weight.

For biomarker extraction ca. 10 g of sediment was freeze dried and mechanically powdered. The sediments were extracted with a Dichloromethane (DCM):Methanol (MeOH) solvent mixture (9:1, v/v, 3 times for 5 min each) using an Accelerated Solvent Extractor (ASE, Dionex 200) at 100°C and ca. 1000 psi. The resulting Total Lipid Extract (TLE) was evaporated to near dryness using a rotary evaporator under near vacuum. The TLE then was transferred to a 4 ml vial and dried under a continuous N_2 flow. A 50% split of the TLE was archived. For the working other half elemental sulfur was removed by adding activated (in 2M HCl) copper turnings to the TLE in DCM and stirring overnight. The TLE was subsequently filtered over Na_2SO_4 to remove the CuS, after which 500 ng of a C_{46} GDGT internal standard was added (Huguet et al., 2006). The resulting TLE was separated over a small column (Pasteur pipette) packed with activated Al_2O_3 (2 h at 150°C). The TLE was separated into an apolar, a ketone and a polar fraction by eluting with n-hexane : DCM 9:1 (v/v), n-hexane : DCM 1:1 (v/v) and DCM : MeOH 1:1 (v/v) solvent mixtures, respectively. The apolar fraction was analyzed by gas chromatography (GC) coupled to a flame ionization detector (FID) and gas chromatography/mass spectroscopy (GC/MS) for quantification and identification of specific biomarkers, respectively. For GC, samples were dissolved in 55 µl hexane and analyzed using a Hewlett Packard G1513A autosampler interfaced to a Hewlett Packard 6890 series Gas Chromatography system equipped with flame ionization detection, using a CP-Sil-5 fused silica capillary column (25 m x 0.32 mm, film thickness 0.12 µm),

359 with a 0.53 mm pre-column. Temperature program: 70°C to 130°C (0 min) at 20°C/min, then
360 to 320°C at 4°C/min (hold time 20 mins). The injection volume of the samples was 1 µl.
361 Analyses of the apolar fractions were performed on a ThermoFinnigan Trace GC ultra,
362 interfaced to a ThermoFinnigan Trace DSQ MS using the same temperature program, column
363 and injection volume as for GC analysis. Alkane ratios are calculated using peak surface areas
364 of the respective alkanes from the GC/FID chromatograms.
365
366 Prior to analyses, the polar fractions, containing the GDGTs, were dissolved in *n*-hexane :
367 propanol (99:1, v/v) and filtered over a 0.45 µm mesh PTFE filter (ø 4mm). Subsequently,
368 analyses of the GDGTs was performed using ultra high performance liquid chromatography-
369 mass spectrometry (UHPLC-MS) on an Agilent 1290 infinity series instrument coupled to a
370 6130 quadrupole MSD with settings as described in Hopmans et al. (2016). In short,
371 separation of GDGTs was performed on two silica Waters Acquity UHPLC HEB Hilic
372 (1.7µm, 2.1mm x 150mm) columns, preceded by a guard column of the same material.
373 GDGTs were eluted isocratically using 82% A and 18% B for 25 mins, and then with a linear
374 gradient to 70% A and 30% B for 25 mins, where A is *n*-hexane, and B = *n*-
375 hexane:isopropanol. The flow rate was constant at 0.2 ml/min. The $[M+H]^+$ ions of the
376 GDGTs were detected in selected ion monitoring mode, and quantified relative to the peak
377 area of the C_{46} GDGT internal standard.
378
379 **5 Results**
380 *5.1 Stable isotope data*
381 The glacial-interglacial range in *Cassidulina teretis* $\delta^{18}O$ ($\delta^{18}O_b$) is ~1‰ between MIS 98 and
382 97, and ~1.3‰ between MIS 95 and 94, but with considerably more variation in especially
383 MIS 95 (Fig. 3). The $\delta^{13}C_b$ data co-vary consistently with $\delta^{18}O_b$ and have a glacial-interglacial

384 range of ~1.1‰, besides one strongly depleted value in MIS 94 (-3.5‰). The MIS 95 $\delta^{13}C_b$
385 values are less variable than the $\delta^{18}O_b$, pointing to an externally forced signal in the latter. The
386 $\delta^{18}O_b$ confirms the relation between glacial stages and fine grained sediment as proposed by
387 Kuhlman et al. (2006a,b). Although the data are somewhat scattered, the A15-3/4 phase
388 relation to the sediment facies is in agreement with the high-resolution stable isotope benthic
389 foraminifera record of the onshore Noordwijk borehole (Noorbergen et al., 2015). The glacial
390 to interglacial ranges are very similar in magnitude with those reported by Sosdian and
391 Rosenthal (2009) for the North Atlantic, but on average lighter by ~0.5‰ ($\delta^{18}O_b$) and ~1.8‰
392 ($\delta^{13}C_b$).
393
394 *5.2 Palynology*
395 Palynomorphs, including dinocysts, freshwater palynomorphs and pollen, are abundant,
396 diverse, and well-preserved in these sediments. Striking is the dominance by conifer pollen.
397 Angiosperm (tree) pollen are present and diverse, but low in abundance relative to conifers.
398 During interglacials (MIS 103, 99, 97, 95, and 93) the pollen record generally shows
399 increased and more diverse tree pollen (particularly *Picea* and *Tsuga*), and warm temperate
400 *Osmunda* spores, whereas during glacials (MIS 102, (100), 98, 96, and 94) herb and heath
401 pollen indicative of open landscapes are dominant (Fig S2). The % arboreal pollen (AP;
402 excluding bisaccate pollen) summarizes these changes, showing maximum values of >40%
403 restricted to just a part of the coarser grained interglacial intervals (Fig. 3). The percentage
404 record of cold water dinocysts is quite scattered in some intervals but indicates generally
405 colder conditions within glacial stages, and minima during %AP maxima (Fig. 3). After peak
406 cold conditions and a TOC maximum (see below), but still well within the glacials, the %
407 Protoperidinoid consistently increases. Some intervals (e.g., top of MIS 94) are marked by
408 influxes of freshwater algae (*Pediastrum* and *Botryococcus)*, indicating a strong riverine

Deleted: .

410 input, these data however do not indicate a clear trend. This robust in-phase pattern of glacial-
411 interglacial variations is also reflected by high T/M ratios during glacials, indicating coastal
412 proximity, and low T/M during (final phases of) interglacials. The Glacial-Interglacial (G-IG)
413 variability in the T/M ratio is superimposed on a long-term increase. The coastal (warm-
414 tolerant) dinocyst maxima are confined to the interglacial intervals and their abundance
415 increases throughout the record. Successive increases of coastal inner neritic *Lingulodinium*
416 *machaerophorum*, followed by increases in coastal lagoonal species in the youngest part,
417 mirror the shoaling trend in the T/M ratio, which in time correspond with the gradual
418 progradation of the Eridanos delta front (Fig. S1).
419
420 *5.3 Organic geochemical proxies*
421 The lowest TOC contents are reached in the clay intervals, and typically range between 0.5%
422 in glacials and 1% in interglacials (Fig. 3). Nitrogen concentrations are relatively stable
423 resulting in C/N ratios primarily determined by organic carbon content, ranging between ~8-9
424 (glacials) and ~14 and 17 (interglacials). The Carbon Preference Index (CPI) is generally
425 high, reflecting a continuous input of immature terrestrial organic matter. Minimum CPI
426 values of ~2.8 - 2.9 are reached at the transitions from the coarser sediments to the clay
427 intervals after which they increase to maxima of 4.5 - 5.0 in the late interglacials. The n-C_{23+25}
428 *Sphagnum* biomarker correlates consistently with the T/M ratio, %AP, and cold water
429 dinocysts (Fig. 3), while the variation in the CPI index is partially out of phase; it is more
430 gradual and lags the % TOC and other signals. Generally lower Branched and Isoprenoid
431 Tetraether (BIT) index values during interglacials (Fig. 3) indicate more marine conditions,
432 i.e. larger distance to the coast and relatively reduced terrestrial input from the Eridanos
433 catchment (cf. Sinninghe Damsté, 2016). As both brGDGT input (run off, soil exposure and
434 erosion) and sea level (distance to the coast) vary across G-IG timescales, for example during

435 deglaciation and subsequent reactivation of fluvial transport (Bogaart and van Balen, 2000),
436 the variability of the BIT index is somewhat different compared to the T/M palynomorph ratio
437 (Fig. 3), but is generally in phase with gradual transitions along G-IG cycles. The MAT_{mr}-
438 based temperature reconstructions vary between 5 and 17°C, reaching maximum values in
439 MIS 97. However, in the MIS 99/98 and MIS 96/95 transitions the MAT_{mr} shows variability
440 opposite to the identified G-IG cycles and the signal contains much high-order variability.
441 Low values during interglacials generally coincide with low CBT'-reconstructed soil pH of
442 <6.0 (Fig. 3).
443
444 *Figure 3: spliced record of A15-3 and A15-4 showing the principal geochemical and*
445 *palynological indices. Shaded blue intervals represent the identified glacial MIS delimited by*
446 *the gamma-ray transitions following Kuhlmann et al. (2006a,b). Data density is dependent on*
447 *type of sample as indicated in Fig. 1. Age scale is based on correlation and LOESS*
448 *interpolation of the identified MIS transitions to the LR04 benthic stack (Lisiecki and Raymo,*
449 *2005) as shown in Fig S3. Data is available in Tables S2 and 3. Red line in the T/M ratio is a*
450 *LOWESS (locally weighted scatterplot smoothing) function with span 0.1.*
451

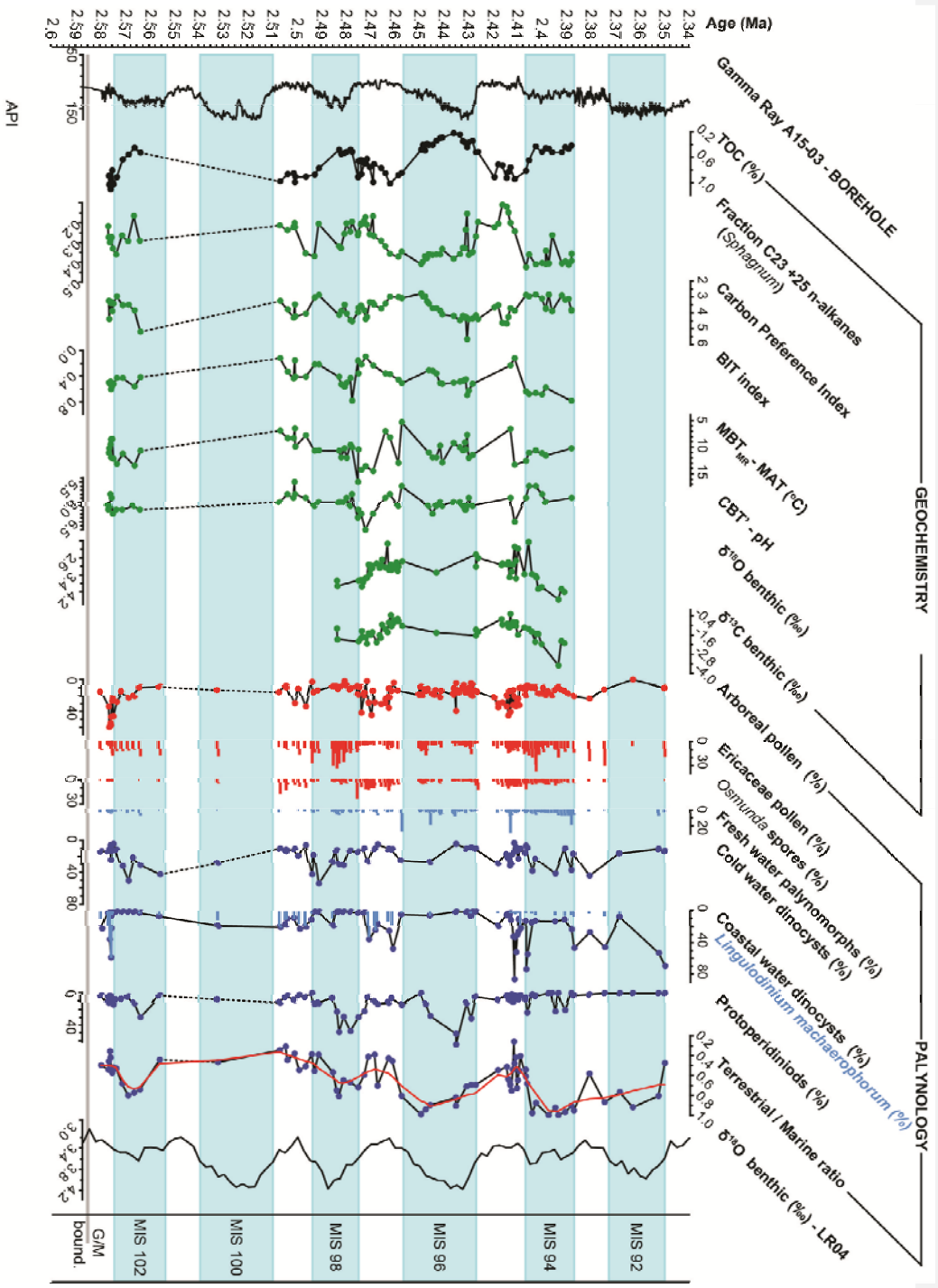
Age (Ma)
API
Gamma Ray A15-03 - BOREHOLE
TOC (%)
Fraction C23 +25 n-alkanes
(Sphagnum)
Carbon Preference Index
BIT Index
MBT5ME' - MAT (°C)
CBT' - pH
δ18O benthic (‰)
δ13C benthic (‰)
Arboreal pollen (%)
Ericaceae pollen (%)
Osmunda spores (%)
Fresh water palynomorphs (%)
Cold water dinocysts (%)
Coastal water dinocysts (%)
Lingulodinium machaerophorum (%)
Protoperidiniods (%)
Terrestrial / Marine ratio
δ18O benthic (‰) - LR04
GEOCHEMISTRY
PALYNOLOGY
G/M bound.
MIS 102
MIS 100
MIS 98
MIS 96
MIS 94
MIS 92

6 Discussion

6.1 Paleoenvironmental setting and climate signals

The source area study by Kuhlmann et al. (2004) indicated the Eridanos paleoriver as the principal source of the terrestrial deposits. The detailed seismic interpretations indeed show the advancing Eridanos delta front from the east toward the sites, especially between 2.44 and 2.34 Ma (Fig. S1). This trend is captured by the long-term increases in the T/M ratio and the proportion of coastal dinocysts (Fig. 3). Bisaccate pollen is the component most sensitive to differential transport processes, yet regardless of whether it is included in the T/M index (Fig. S5) the same patterns are recorded, indicating no direct influence of differential transport on the T/M ratio in this dataset. During MIS 103, 99, 97, 95, and 93 the AP% increases indicate generally warmer and more humid conditions than during MIS 102, 98, 96, and 94 (Fig. 3). The cold-water temperature signal based on dinocysts is more variable than the terrestrial cooling signals from the AP%. Pollen assemblages represent mean standing vegetation in the catchment, and also depend on dominant circulation patterns and short-term climate variations (Donders et al., 2009). Due to exclusion of bisaccate pollen, the %AP is generally low but eliminates any climate signal bias due to the direct effect of sea level changes (Donders et al., 2009; Kotthoff et al., 2014). In the record there are small but significant time lags between proxies, which have important implications for explaining the forcing of G-IG cycles. In the best constrained MIS transition (98 to 97), the G-IG transition is seen first in decreases of the cold water dinocysts and *n*-C_{23+25} n-alkanes predominantly derived from *Sphagnum*. Subsequently the BIT decreases, and MAT_{mr} and the %AP increase, and finally the $\delta^{18}O_b$ and T/M ratio decrease with a lag of a few thousand years (Fig. 3). Changes in the CPI record are more gradual, but generally in line with T/M. The AP% and T/M proxies have the most extensive record and detailed analysis of several glacial-interglacial transitions shows that the declines in AP% consistently lead the T/M increases by 3-8 kyr based on the present age

Deleted: In- or exclusion of bisaccate pollen in the T/M index (Fig. S5), the component most sensitive to differential transport processes, indicates no direct influence of differential transport on the T/M ratio

model (Fig. S2). The T/M ratio variability corresponds well to the LR04 benthic stack (Fig. 3), which is primarily an obliquity signal. Within the constraints of the sample availability, our record captures the approximate symmetry between glaciation and deglaciation typical of the Early Pleistocene (Lisiecki and Raymo, 2005).

The high variability and strongly depleted values in $\delta^{18}O_b$ during MIS 95 occur during peak coastal dinocyst abundances, suggesting high run off during maximum warming phases. During cold water dinocysts maxima, the high abundance of Protoperidinioids indicates high nutrient input, and productive spring/summer blooms, which point to strong seasonal temperature variations. This productivity signal markedly weakens in MIS 94 and 92 and the gradual T/M increase is consistent with the basin infill and gradually approaching shelf-edge delta (Fig. S1). As Protoperidinioid minima generally occur during TOC maxima there is no indication for a preservation overprint since selective degradation typically lowers relative abundances of these P-cysts (Gray et al., 2017). Combined, the high TOC and CPI values, coastal and stratified water conditions, and intervals of depleted $\delta^{18}O_b$ document increased Eridanos run-off during interglacials. These suggest a primarily terrestrial organic matter source that, based on mineral provenance studies (Kuhlmann et al., 2004) and high conifer pollen abundance documented here, likely originated from the Fennoscandian Shield. The fine-grained material during cold phases is probably transported by meltwater during summer from local glaciers that developed since the late Pliocene at the surrounding Scandinavian mainland (Mangerud et al., 1996; Kuhlmann et al., 2004).

6.2 Temperature reconstruction and brGDGT input

509 Whereas the BIT index reflects the G-IG cycles consistently, the MAT_{mr} record, which is
510 based on GDGTs, has a variable phase relation with the G-IG cycles and high variability. The
511 use of MAT_{mr} in coastal marine sediments is based on the assumption that river-deposited
512 brGDGTs reflect an integrated signal of the catchment area. As the Eridanos system is
513 reactivated following glacials, glacial soils containing brGDGT are likely eroded causing a
514 mixed signal of glacial and interglacial material. The lowest MAT_{mr} and highest variability is
515 indeed observed during periods of deposition of sediments with a higher TOC content and
516 minima of CBT'-derived pH below 6 (Fig. 3), consistent with increased erosion of acidic
517 glacial (peat) soil. Additional analysis of the apolar fractions in part of the samples reveals
518 during these periods a relatively high abundance of the C_{31} 17α, 21β-homohopanes, which in
519 immature soils indicates a significant input of acidic peat (Pancost et al., 2002). This suggests
520 that the variability in the MAT_{mr} record is not fully reliable due to (variable) erosion of glacial
521 soils or peats. Alternatively, the terrestrial brGDGT signal may be altered by a contribution of
522 brGDGTs produced in the marine realm. BrGDGTs were initially believed to be solely
523 produced in soils, but emerging evidence suggests that brGDGTs are also produced in the
524 river itself (e.g., Zell et al., 2013; De Jonge et al., 2014b) and in the coastal marine sediments
525 (e.g., Peterse et al., 2009; Sinninghe Damsté, 2016) Based on the modern system, the degree
526 of cyclisation of tetramethylated brGDGTs ($\#rings_{tetra}$) has been proposed to identify a
527 possible in situ overprint (Sinninghe Damsté, 2016). The $\#rings_{tetra}$ in this sediment core is
528 <0.37, which is well below the suggested threshold of 0.7, and thus suggests that the
529 brGDGTs are primarily soil-derived. However, a ternary diagram of the brGDGT distribution
530 show some offset to the global soil calibration that decreases with increasing BIT values (Fig.
531 S6), pointing to some influence of in-situ GDGT production when terrestrial input is
532 relatively low. Finally, selective preservation in the catchment and during fluvial transport
533 may have affected the brGDGT signal, although experimental evidence on fluvial transport

processes indicates that these do not significantly affect initial soil-brGDGT compositions (Peterse et al., 2015).

6.3 Implications for the intensification of Northern Hemisphere glaciations

The classic Milankovitch model predicts that global ice volume is forced by high northern summer insolation (e.g. Hays et al., 1976). Raymo et al. (2006) suggested an opposite response of ice sheets on both hemispheres due to precession forcing, cancelling out the signal and amplifying obliquity in the early Pleistocene. That hypothesis predicts that regional climate records on both hemispheres should contain a precession component that is not visible in the sea level and deep sea $\delta^{18}O_b$ record, and is supported by evidence from Laurentide Ice Sheet melt and iceberg-rafted debris of the East Antarctic ice sheet (Patterson et al., 2014; Shakun et al., 2016). Alternatively, a dominantly obliquity forced G-IG cycle is supported by a significant temperature component in the temperature deep sea $\delta^{18}O_b$ record (Sosdian and Rosenthal, 2009) and dominant 41-kyr variability in North American biomarker dust fluxes. Our results show that the regional NH climate on both land and sea surface vary on the same timescale as the local relative sea level which, with the best possible age information so far (Fig. S3), mirrors the global LR04 $\delta^{18}O_b$ record. The temperature changes lead the local sea level by 3-8 kyr, which is consistent with a NH obliquity forcing scenario as cooling would precede ice buildup and sea level change. Contrary to the model proposed by Raymo et al. (2006), this suggests that the NH obliquity forcing is the primary driver for the glacial-interglacial in the early Pleistocene, although we cannot exclude precession forcing as a contributing factor.. Various studies indicate the importance of gradual CO_2 decline in the intensification of NHG (Kürschner et al., 1996; Seki et al., 2010; Bartoli et al., 2011) combined with the threshold effects of ice albedo (Lawrence et al., 2010; Etourneau et al.,

Deleted: C

559 2010) and land cover changes (Koenig et al., 2011). Simulations of four coupled 3-D ice
560 models indicate that Antarctic ice volume increases respond primarily to sea-level lowering,
561 while Eurasian and North American ice sheet growth is initiated by temperature decrease (de
562 Boer et al., 2012). The latter dominate the eustatic sea-level variations during glacials. Our
563 observations agree with the modelled temperature sensitivity of NH ice sheet growth. The
564 dominant obliquity signal further suggests a seasonal aspect of the climate forcing. The
565 combination of high summer productivity, based on increased Protoperidiniod dinocysts, and
566 increased proportions of cold dinocysts during the glacials in the SNS record indicate a strong
567 seasonal cycle. This confirms similar results from the North Atlantic (Hennissen et al., 2015)
568 and is consistent with an obliquity-driven glacial-interglacial signal in a mid-latitudinal
569 setting, likely promoting meridional humidity transport and ice buildup.

570

571 The southward migration of Arctic surface water masses indicated by increases in cold water
572 dinocysts (Fig. 3) is furthermore relevant for understanding the relation between the Atlantic
573 meridional overturning circulation (AMOC) intensity and ice sheet growth (e.g. Bartoli et al.,
574 2005; Naafs et al, 2010). Mid-Pliocene increased heat transport and subsequent decrease
575 during NHG due to AMOC intensity changes has been invoked from many proxy records but
576 is difficult to sustain in models (Zhang et al., 2013). Our results indicate that the NW
577 European early Pleistocene climate experienced significant cooling in all temperature-
578 sensitive proxies during sea-level lowstands, which is consistent with southward displacement
579 of the Arctic front and decreased AMOC (Naafs et al., 2010). The MAT_{mr} indicates a 4-6 ^{o}C
580 glacial-interglacial amplitude although the timing is offset relative to the other proxies. The
581 data-model mismatch in AMOC changes might be due to dynamic feedbacks in vegetation or
582 (sea-) ice (Koenig et al., 2011; de Boer et al., 2012) that are prescribed variables in the model
583 comparison by Zhang et al. (2013).

584

585 In addition, our SNS record provides a well-dated early Pleistocene Glacial-Interglacial
586 succession integrating marine and terrestrial signals improving on the classic terrestrial
587 Praetiglian stage. While conceptually valid, the earliest Pleistocene glacial stages defined in
588 the continental succession of the SE Netherlands (Van der Vlerk and Florschütz, 1953;
589 Zagwijn, 1960) and currently considered text book knowledge, are highly incomplete and
590 locally varied (Donders et al., 2007). This shallow marine SNS record provides a much more
591 suitable reflection of large-scale transitions and trends in NW Europe and merits further
592 development by complete recovery of the sequence in a scientific drilling project (Westerhoff
593 et al., 2016).

594

595 **7 Conclusions**

596 The independently dated late Pliocene-early Pleistocene sedimentary succession of the
597 southern North Sea Basin provides a record that straddles the intensification of Northern
598 Hemisphere Glaciation and the subsequent climate fluctuations in a shallow marine setting in
599 great detail. The intensification of the glaciation and the correlation to marine isotope stages
600 103 to 92, including the conspicuous first Pleistocene glacial stages 98, 96 and 94, is well
601 expressed in the marine and terrestrial palynomorph and organic biomarker records of the
602 southern North Sea. The independent relative sea- and land-based temperature records show
603 clearly coeval (at this resolution) expression of glacial-interglacial and sea-level cycles that
604 are well-correlated to the LR04 benthic stack. Critically, both the biomarker signals, %AP,
605 and cold water dinocyst variations show consistent in-phase variability on obliquity time
606 scales, leading sea-level changes by 3-8 kyr, which supports a dominantly direct NH
607 insolation control over early Pleistocene glaciations. Based on this integrated record, NH

obliquity forcing is the primary driver for the glacial-interglacial cycles in the early Pleistocene. Furthermore, our findings support the hypothesis of temperature sensitivity of NH ice sheet growth. The interglacials are characterized by (seasonally) stratified waters and/or near-shore conditions as glacial-interglacial cycles became more expressive and the Eridanos delta progressed into the region. The strong seasonality at mid-latitudes point to a vigorous hydrological cycling that should be considered as a potential factor in ice sheet formation in further investigations.

8 Author contributions

THD, HB and GK designed the research. NvH carried out the geochemical analyses under supervision of JW, GJR, FP and JSSD. RV, DM and THD carried out the palynological analyses and interpreted the data together with FS. LL and RPS provided stable isotope data on benthic foraminifera. JtV provided seismic interpretations. THD integrated the data and wrote the paper with contributions from all authors.

9 Acknowledgements

We are grateful the constructive comments of Stijn de Schepper and David Naafs and an anonymous referee that helped to improve the manuscript. We gratefully acknowledge the support in providing the offshore samples to this study and permission to publish by Wintershall Noordzee B.V., and project support by partners Chevron Exploration and Production Netherlands B.V., Total E&P Nederland B.V., Dana Petroleum Netherlands B.V., Oranje-Nassau Energie B.V., and Energie Beheer Nederland (EBN). Arnold van Dijk is thanked for running C/N and stable isotope analyses, and Giovanni Dammers for processing

palynological samples. The work was partly supported by funding from the Netherlands Earth System Science Center (NESSC) through a gravitation grant (NWO 024.002.001) from the Dutch Ministry for Education, Culture and Science to JSSD, GJR, and LL.

10 References

Baas, M., Pancost, R., van Geel, B. Sinninghe Damsté, J.S., 2000. A comparative study of lipids in *Sphagnum* species. Organic Geochemistry 31: 535-539. https://doi.org/10.1016/S0146-6380(00)00037-1

Bakken, K. and Dale, B., 1986. Dinoflagellate cysts in Upper Quaternary sediments from southwestern Norway and potential correlations with the oceanic record. Boreas 15: 185-190. DOI: 10.1111/j.1502-3885.1986.tb00082.x

Bartoli, G., Hönisch, B., Zeebe, R.E., 2011. Atmospheric CO_2 decline during the Pliocene intensification of Northern Hemisphere glaciations. Paleoceanography 26, PA4213. http://dx.doi.org/10.1029/2010PA002055.

Bijlsma, S., 1981. Fluvial sedimentation from the Fennoscandian area into the Northwest European Basin during the Late Cenozoic. Geologie en Mijnbouw 60: 337-345.

Bogaart, P.W., van Balen, R.T., 2000. Numerical modeling of the response of alluvial rivers to Quaternary climate change. Global and Planetary Change 27: 147-163. https://doi.org/10.1016/S0921-8181(01)00064-9

Bray, E.E., and Evans, E.D., 1961. Distribution of n-parrafins as a clue to recognition of source beds. Geochimica et Cosmochimica Acta 22: 2-15. https://doi.org/10.1016/0016-7037(61)90069-2

Brierley, C.M., and Fedorov, A.V., 2010. Relative importance of meridional and zonal sea surface temperature gradients for the onset of the ice ages and Pliocene - Pleistocene climate evolution. Paleoceanography 25: PA2214. DOI:10.1029/2009PA001809.

Brigham-Grette, J, Melles, M., Minyuk, P.S., Andreev, A.A., Tarasov, P.E., DeConto, R.M., König, S. Nowaczyk, N.R., Wennrich, V., Rosén, P., Haltia-Hovi, E., Cook, T.L., Gebhardt, C., Meyer-Jacob, C., Snyder, J.A., Herzschuh, U., 2013. Pliocene warmth, polar amplification, and stepped Pleistocene cooling recorded in NE Arctic Russia. Science 340: 1421-1427. DOI: 10.1126/science.1233137

Caston, V.N.D., 1979. The Quaternary sediments of the North Sea. In: Banner, F.T., Collins, M.B., Massie, K.S. (Eds.), The north-west European shelf seas: the sea bed and the sea in motion. I. Geology and Sedimentology, Elsevier Oceanographic Series 24A, p. 195-270.

Field Code Changed

Dale, B., 1996. Dinoflagellate cyst ecology: modelling and geological applications. In: J.M.G. Jansonius, D.C. (Editor), Palynology: Principles and Application, vol. 3. American Association of Stratigraphic Palynologists Foundation, College Station, TX: 1249-1275.

de Boer, B., van de Wal, R.S.W., Lourens, L.J., Bintanja, R., Reerink, T.J., 2012. A continuous simulation of global ice volume over the past 1 million years with 3-D ice-sheet models. Climate Dynamics 41, 1365. doi:10.1007/s00382-012-1562-2

de Haas, H., Boer, W., van Weering, T.C.E., 1997. Recent sediment and organic carbon burial in a shelf sea; the North Sea. Marine Geology 144, 131–146. https://doi.org/10.1016/S0025-3227(97)00082-0.

De Jonge, C,.Hopmans, A.C, Zell, C.I., Kim, J.-H., Schouten, S., Sinninghe Damsté, J.S., 2014a. Occurrence and abundance of 6-methyl branched glycerol dialkyl glycerol tetraethers in soils: Implications for palaeoclimate reconstruction. Geochimica et Cosmochimica Acta 141: 97-112. https://doi.org/10.1016/j.gca.2014.06.013.

De Jonge. C., Stadnitskaia, A., Hopmans, E.C., Cherkashov, G., Fedotov, A. and Sinninghe Damsté, J.S., 2014b. In-situ produced branched glycerol dialkyl glycerol tetraethers in suspended particulate matter from the Yenisei River, Eastern Siberia. Geochimica et Cosmochimica Acta 125: 476-491. https://doi.org/10.1016/j.gca.2014.06.013.

De Schepper, S., Head, M.J., and Louwye, S., 2009. Pliocene dinoflagellate cyst stratigraphy, palaeoecology and sequence stratigraphy of the Tunnel-Canal Dock, Belgium, Geological Magazine 146: 92-112. DOI: 10.1017/S0016756808005438.

De Schepper, S., Fischer, E.I., Groeneveld, J., Head, M.J., Matthiessen, J., 2011. Deciphering the palaeoecology of Late Pliocene and Early Pleistocene dinoflagellate cysts. Palaeogeography, Palaeoclimatology, Palaeoecology 309: 17–32. https://doi.org/10.1016/j.palaeo.2011.04.020.

De Schepper, S., Groeneveld, J., Naafs, B.D.A., Van Renterghem, C., Hennissen, J., Head, M.J., Louwye, S., Fabian, K., 2013. Northern Hemisphere glaciation during the globally warm early Late Pliocene. PLoS ONE 8 (12), e81508. http://dx.doi.org/10.1371/journal.pone.0081508.

de Vernal, A., 2009. Marine palynology and its use for studying nearshore environments, From Deep-Sea to Coastal Zones: Methods – Techniques for Studying Paleoenvironments, IOP Conference Series: Earth and Environmental Science, 5, 012002.DOI:10.1088/1755-1307/5/1/012002.

Donders, T.H., Kloosterboer-van Hoeve, M.L., Westerhoff, W., Verreussel, R.H.C.M. & Lotter, A.F., 2007. Late Neogene continental stages in NW Europe revisited. Earth-Science Reviews 85: 161-186. https://doi.org/10.1016/j.earscirev.2007.06.004.

Donders, T.H., Weijers, J.W.H., Munsterman, D.K., Kloosterboer-van Hoeve, M.L., Buckles, L.K., Pancost, R.D., Schouten, S., Sinninghe Damsté, J.S. & Brinkhuis, H., 2009. Strong

climate coupling of terrestrial and marine environments in the Miocene of northwest Europe. Earth and Planetary Science Letters 281 (3-4): 215-225. https://doi.org/10.1016/j.epsl.2009.02.034.

Eglinton, G., Hamilton, R.J., 1967. Leaf epicuticular waxes. Science 156, 1322-1335. DOI: 10.1126/science.156.3780.1322.

Etourneau, J., Schneider, R., Blanz, T., Martinez, P., 2010. Intensification of the Walker and Hadley atmospheric circulations during the Pliocene-Pleistocene climate transition. Earth and Planetary Science Letters 297: 103-110. http://dx.doi.org/10.1016/j.epsl.2010.06.010.

Faegri, K., Iversen, J., Kaland, P.E., Krzywinski, K., 1989. Text book of pollen analysis, IV Edition. The Blackburn Press, 328 pp.

Gibbard P.L., and Lewin, J., 2016. Filling the North Sea Basin: Cenozoic sediment sources and river styles. Geologica Belgica 19: 201-217. http://dx.doi.org/10.20341/gb.2015.017

Gray, D. D., Zonneveld, K.A., & Versteegh, G.J., 2017. Species-specific sensitivity of dinoflagellate cysts to aerobic degradation: A five-year natural exposure experiment. Review of Palaeobotany and Palynology 247, 175-187. DOI: 10.1016/j.revpalbo.2017.09.002

Head, M.J., 1996. Modern dinoflagellate cysts and their biological affinities. In: Jansonius, J., McGregor, D.C. (Eds.), Palynology: Principles and Application, vol. 3. American Association of Stratigraphic Palynologists Foundation, College Station, TX, pp. 1197-1248.

Haug, G.H. and Tiedemann, R., 1998. Effect of the formation of the Isthmus of Panama on Atlantic Ocean thermohaline circulation. Nature 393 (6686): 673- 676. DOI:10.1038/31447.

Haug, G.H., Sigman, D.M., Tiedemann, R., Pedersen, T.F. & Sarnthein, M., 1999. Onset of permanent stratification in the subarctic Pacific Ocean. Nature 40: 779–782. DOI:10.1038/44550

Haug, G.H., Ganopolski, A., Sigman, D.M., Rosell-Mele, A., Swann, G. E. A, Tiedemann, R., Jaccard, S. L., Bollmann, J., Maslin, M.A., Leng, M.J. and Eglinton, G., 2005. North Pacific seasonality and the glaciation of North America 2.7 million years ago. Nature 433: 821-825. DOI: 10.1038/nature03332.

Hays, J. D., Imbrie, J. & Shackleton, N. J., 1976. Variations in the Earth's orbit: pacemaker of the ice ages. Science 194; 1121–1132. doi: 10.1126/science.194.4270.1121.

Head, M.J., Riding, J.B., Eidvin, T., Chadwick, R.A., 2004. Palynological and foraminiferal biostratigraphy of (Upper Pliocene) Nordland Group mudstones at Sleipner, northern North Sea. Marine and Petroleum Geology 21:277-297. http://dx.doi.org/10.1016/j.marpetgeo.2003.12.002.

Hedges, J.I., Keil, R.G., & Benner, R., 1997. What happens to terrestrial organic matter in the ocean? Organic Geochemistry 27: 195-212. https://doi.org/10.1016/S0146-6380(97)00066-1

Hennissen, J.A.I., Head, M.J., De Schepper, S., Groeneveld, J., 2015. Increased seasonality during the intensification of Northern Hemisphere glaciation at the Pliocene-Pleistocene transition ~2.6 Ma. Quaternary Science Reviews 129: 321–332. https://doi.org/10.1016/j.quascirev.2015.10.010.

Hennissen, J.A.I., Head, M.J., De Schepper, S., Groeneveld, J., 2017. Dinoflagellate cyst paleoecology during the Pliocene–Pleistocene climatic transition in the North Atlantic. Palaeogeography, Palaeoclimatology, Palaeoecology 470: 81-108. https://doi.org/10.1016/j.palaeo.2016.12.023.

Heusser, L.E., and Shackleton, N.J., 1979. Direct marine-continental correlation: 150,000-year oxygen isotope-pollen record from the North Pacific. Science 204: 837-839. DOI: 10.1126/science.204.4395.837.

Hooghiemstra, H., 1988. Palynological records from Northwest African marine sediments: a general outline of the interpretation of the pollen signal. Philosophical Transactions of the Royal Society of London, Series B Biological Sciences 318 (1191): 431–449. DOI: 10.1098/rstb.1988.0018.

Hooghiemstra, H., Ran, E.T.H., 1994. Late Pliocene-Pleistocene high resolution pollen sequence of Colombia: An overview of climatic change. Quaternary International, 21: 63-80

Hopmans, E.C., Weijers, J.W.H., Schefuss, E., Herfort, L., Sinninghe Damsté, J.S., Schouten, S., 2004. A novel proxy for terrestrial organic matter in sediments based on branched and isoprenoid tetraether lipids. Earth and Planetary Science Letters 24: 107–116. https://doi.org/10.1016/j.epsl.2004.05.012.

Hopmans, E.C., Schouten, S., Sinninghe Damsté, J.S., 2016. The effect of improved chromatography on GDGT-based palaeoproxies. Organic Geochemistry 93: 1-6. https://doi.org/10.1016/j.orggeochem.2015.12.006.

Huuse, M., Lykke-Andersen, H., Michelsen, O., 2001. Cenozoic evolution of the eastern North Sea Basin – new evidence from high-resolution and conventional seismic data. Marine Geology 177: 243-269.

Huybers, P., 2011. Combined obliquity and precession pacing of late Pleistocene deglaciations. Nature 480: 229–232. DOI:10.1038/nature10626.

Keigwin, L. D., 1982. Isotope paleoceanography of the Caribbean and east Pacific: role of Panama uplift in late Neogene time. Science 217: 350–353. DOI: 10.1126/science.217.4557.350.

Kemna, H.A., Westerhoff, W.E., 2007. Remarks on the palynology-based chronostratigraphic subdivision of the Pliocene terrestrial deposits in NW-Europe. Quaternary International 164–165: 184–196. https://doi.org/10.1016/j.quaint.2006.10.017.

Field Code Changed

771 Kennicutt II, M.C., Barker, C., Brooks, J.M., DeFreitas, D.A., Zhu, G.H., 1987. Selected
772 organic matter source indicators in the Orinoco, Nile and Changjiang deltas. Organic
773 Geochemistry 11: 41-51. https://doi.org/10.1016/0146-6380(87)90050-7.

774 Knies, J., Cabedo-Sanz, P., Belt, S.T., Baranwal, S., Fietz, S., Rosell-Mele, A., 2014. The
775 emergence of modern sea ice cover in the Arctic Ocean. Nature Communications 5:
776 http://dx.doi.org/10.1038/ncomms6608.

777 Koenig, S.J., DeConto, R.M. & Pollard, D., 2011. Late Pliocene to Pleistocene sensitivity of
778 the Greenland Ice Sheet in response to external forcing and internal feedbacks. Climate
779 Dynamics 37: 1247. DOI:10.1007/s00382-011-1050-0.

780 Kotthoff, U., Greenwood, D., McCarthy, F., Müller-Navarra, K., Prader, S., Hesselbo, S.,
781 2014. Late Eocene to middle Miocene (33 to 13 million years ago) vegetation and climate
782 development on the North American Atlantic Coastal Plain (IODP Expedition 313, Site
783 M0027). Climate of the Past 10: 1523-1539. https://doi.org/10.5194/cp-10-1523-2014.

784 Kuhlmann, G. & Wong, T.E., 2008. Pliocene paleoenvironment evolution as interpreted
785 from 3D-seismic data in the southern North Sea, Dutch offshore sector. Marine and Petroleum
786 Geology 25: 173-189. https://doi.org/10.1016/j.marpetgeo.2007.05.009.

787 Kuhlmann, G., Pedersen, R.-B., de Boer, P., Wong, T.E., 2004. Provenance of Pliocene
788 sediments and paleoenvironmental change in the southern North Sea region using Sm/Nd
789 (samarium-neodymium) provenance ages and clay mineralogy. Sedimentary Geology 171:
790 205-226. DOI: 10.1016/j.sedgeo.2004.05.016.

791 Kuhlmann, G., Langereis, C.G., Munsterman, D., van Leeuwen, R.-J., Verreussel, R.,
792 Meulenkamp, J., Wong, T.E., 2006a. Chronostratigraphy of Late Neogene sediments in the
793 southern North Sea Basin and paleoenvironmental interpretations. Palaeogeography,
794 Palaeoclimatology, Palaeoecology 239: 426–455.
795 https://doi.org/10.1016/j.palaeo.2006.02.004.

796 Kuhlmann, G., Langereis, C.G., Munsterman, D., van Leeuwen, R.-J., Verreussel, R.,
797 Meulenkamp, J.E., Wong, Th.E., 2006b. Integrated chronostratigraphy of the Pliocene–
798 Pleistocene interval and its relation to the regional stratigraphical stages in the southern North
799 Sea region. Netherlands Journal of Geosciences - Geologie en Mijnbouw 85 (1): 19–35.
800 https://doi.org/10.1017/S0016774600021405.

801 Kürschner, W.A., van der Burgh, J., Visscher, H., and Dilcher, D.L., 1996. Oak leaves as
802 biosensors of late Neogene and early Pleistocene paleoatmospheric CO_2 concentrations.
803 Marine Micropaleontology 27: 299-312. https://doi.org/10.1016/0377-8398(95)00067-4.

804 Larsson, L.M., Dybkjaer, K., Rasmussen, E.S., Piasecki, S., Utescher, T., and Vajda, V.,
805 2011. Miocene climate evolution of northern Europe: A palynological investigation from
806 Denmark. Palaeogeography, Palaeoclimatology, Palaeoecology 309: 161-175.
807 https://doi.org/10.1016/j.palaeo.2011.05.003.

808 Lawrence, K.T., Sosdian, S., White, H.E., Rosenthal, Y., 2010. North Atlantic climate
809 evolution through the Plio-Pleistocene climate transitions. Earth and Planetary Science Letters
810 300: 329-342. http://dx.doi.org/10.1016/j.epsl.2010.10.013.

811 Lisiecki, L.E., and Raymo, M.E., 2005. A Pliocene-Pleistocene stack of 57 globally
812 distributed benthic $\delta^{18}O$ records. Paleoceanography 20: PA1003.
813 DOI:10.1029/2004PA001071.

814 Lister, A.M., 2004. The impact of Quaternary Ice Ages on mammalian evolution.
815 Philosophical Transactions of the Royal Society of London, Series B Biological Sciences 359,
816 221-241. DOI: doi: 10.1098/rstb.2003.1436.

817 Mackensen, A. & Hald, M., 1988. *Cassidulina teretis* Tappan and *C. laevigata* d'Orbigny:
818 their modern and late Quaternary distribution in northern seas. Journal of Foraminiferal
819 Research 18 (1): 16-24. DOI: https://doi.org/10.2113/gsjfr.18.1.16.

820 Mangerud, J., Jansen, E., Landvik, J., 1996. Late Cenozoic history of the Scandinavian and
821 Barents Sea ice sheets. Global and Planetary Change 12: 11-26. https://doi.org/10.1016/0921-
822 8181(95)00009-7.

823 Maslin, M.A., Li, X. S., Loutre M. F., & Berger A. 1998. The contribution of orbital forcing
824 to the progressive intensification of Northern Hemisphere Glaciation. Quaternary Science
825 Reviews 17: 411-426. https://doi.org/10.1016/S0277-3791(97)00047-4.

826 McCarthy, F.M.G. and Mudie, P., 1998. Oceanic pollen transport and pollen:dinocyst ratios
827 as markers of late Cenozoic sea level change and sediment transport. Palaeogeography,
828 Palaeoclimatology, Palaeoecology 138: 187-206. https://doi.org/10.1016/S0031-
829 0182(97)00135-1.

830 Meijer, T., Cleveringa, P., Munsterman, D.K., and Verreussel, R.M.C.H., 2006. The Early
831 Pleistocene Praetiglian and Ludhamian pollen stages in the North Sea Basin and their
832 relationship to the marine isotope record. Journal of Quaternary Science 21: 307–310. DOI:
833 10.1002/jqs.956.

834 Meloro, C., Raia, P., Carotenuto, F., Barbera, C., 2008. Diversity and turnover of Plio-
835 Pleistocene large mammal fauna from the Italian Peninsula. Palaeogeography,
836 Palaeoclimatology, Palaeoecology 268: 58-64. https://doi.org/10.1016/j.palaeo.2008.08.002.

837 Michelsen, O., Thomsen, E., Danielsen, M., Heilmann-Clausen, C., Jordt, H., Laursen, G-V.,
838 1998. Cenozoic sequence stratigraphy in eastern North Sea. In: P.-C. de Graciansky, T.
839 Jacquin, P.R. Vail and M.B. Farley (Eds), Mesozoic and Cenozoic sequence stratigraphy of
840 European Basins: SEPM (Society for Sedimentary Geology) Special Publications 60, 91-118.
841 DOI: https://doi.org/10.2110/pec.98.02.0091.

842 Mudelsee, M. and Raymo, M.E., 2005. Slow dynamics of the Northern Hemisphere
843 glaciation. Paleoceanography 20, PA4022. DOI: 10.1029/2005PA001153.

844 Mudie, P.J. and McCarthy, F.M.G., 1984. Late Quaternary pollen transport processes, western
845 North Atlantic: Data from box models, cross-margin and N-S transects. Marine Geology, 118:
846 79-105. https://doi.org/10.1016/0025-3227(94)90114-7.

847 Naafs, B.D.A., Stein, R., Hefter, J., Khelifi, N., De Schepper, S., Haug, G.H., 2010. Late
848 Pliocene changes in the North Atlantic current. Earth and Planetary Science Letters 298: 434-
849 442. http://dx.doi.org/10.1016/j.epsl.2010.08.023.

850 Naafs, B.D.A., Hefter, J., Acton, G., Haug, G.H., Martínez-Garcia, A., Pancost, R., Stein, R.,
851 2012. Strengthening of North American dust sources during the late Pliocene (2.7 Ma). Earth
852 and Planetary Science Letters 317-318. 8-19, doi:10.1016/j.epsl.2011.11.026

853 Naafs, B.D.A., Hefter, J., Stein, R., 2013. Millennial-scale ice rafting events and Hudson
854 Strait Heinrich(-like) Events during the late Pliocene and Pleistocene: a review. Quaternary
855 Science Reviews 80: 1-28. doi: 10.1016/j.quascirev.2013.08.014.

856 Nichols, J.E., Booth, R.K., Jackson, S.T., Pendall, E.G. & Huang, Y., 2006. Paleohydrologic
857 reconstruction based on n-alkane distributions in ombrotrophic peat. Organic Geochemistry
858 37: 1505-13. https://doi.org/10.1016/j.orggeochem.2006.06.020.

859 Noorbergen, L.J., Lourens, L.J., Munsterman, D. K., Verreussel, R.M.C.H., 2015. Stable
860 isotope stratigraphy of the early Quaternary of borehole Noordwijk, southern North Sea
861 .Quaternary International 386: 148 – 157. DOI:10.1016/j.quaint.2015.02.045.

862 Overeem, I., Weltje, G. J., Bishop-Kay, C., and Kroonenberg, S. B., 2001. The Late Cenozoic
863 Eridanos delta system in the Southern North Sea Basin: a climate signal in sediment supply?
864 Basin Research 13: 293-312. DOI: 10.1046/j.1365-2117.2001.00151.x.

865 Pagani, M., Liu, Z., LaRiviere, J., Ravelo, A.C., 2010. High Earth-system climate sensitivity
866 determined from Pliocene carbon dioxide concentrations. Nature Geoscience. 3: 27-30.
867 http://dx.doi.org/10.1038/NGEO724.

868 Pancost, R.D., Baas, M., van Geel, B., and Sinninghe Damsté, J.S., 2002. Biomarkers as
869 proxies for plant inputs to peats: an example from a sub-boreal ombrotrophic bog. Organic
870 Geochemistry 33(7): 675-690.

871 Pancost, R.D., Baas, M., van Geel, B., and Sinninghe Damsté, J.S., 2003. Response of an
872 ombrotrophic bog to a regional climate event revealed by macrofossil, molecular and carbon
873 isotopic data. The Holocene, 13(6): 921-932. https://doi.org/10.1016/S0146-6380(02)00048-7.

874 Patterson, M.O., McKay, R., Naish, T., Escutia, C., Jimenez-Espejo, F.J., Raymo,
875 M.E.,Meyers, S.R., Tauxe, L., Brinkhuis, H. & IODP Expedition 318 Scientists 2014. Orbital
876 forcing of the East Antarctic ice sheet during the Pliocene and Early Pleistocene. Nature
877 Geoscience 7: 841. DOI: 10.1038/ngeo2273.

878 Peterse, F., Moy, C.M., and Eglinton, T.I., 2015. A laboratory experiment on the behaviour of
879 soil-derived core and intact polar GDGTs in aquatic environments. Biogeosciences 12: 933–
880 943. DOI:10.5194/bg-12-933-2015.

881 Peterse, F., Kim, J.-H., Schouten, S., Kristensen, D.K., Koç, N. & Sinninghe Damsté, J.S.
882 2009. Constraints on the application of the MBT/CBT palaeothermometer at high latitude
883 environments (Svalbard, Norway). Organic Geochemistry 40 (6): 692-699.
884 https://doi.org/10.1016/j.orggeochem.2009.03.004.

885 Poore, H.R., Samworth, R., White, N.J., Jones, S.M., McCave, I.N., 2006. Neogene overflow
886 of Northern Component Water at the Greenland–Scotland Ridge. Geochemistry Geophysics
887 Geosystems 7. http://dx.doi.org/10.1029/2005gc001085.Q06010.

888 Pross, J. and Brinkhuis, H., 2005. Organic-walled dinoflagellate cysts as paleoenvironmental
889 indicators in the Paleogene; a synopsis of concepts. Paläontologische Zeitschrift, 79(1): 53-
890 59.

891 Quaijtaal, W., Donders, T.H., Persico, D. & Louwye, S., 2014. Characterising the middle
892 Miocene Mi-events in the Eastern North Atlantic realm - A first high-resolution marine
893 palynological record from the Porcupine Basin. Palaeogeography, Palaeoclimatology,
894 Palaeoecology 399: 140-159. https://doi.org/10.1016/j.palaeo.2014.02.017.

895 Ravelo, A.C., Andreasen, D.H., Lyle, M., Lyle, A.O., Wara, M.W., 2004. Regional climate
896 shifts caused by gradual global cooling in the Pliocene epoch. Nature 429 (6989): 263-267.
897 DOI:10.1038/nature02567

898 Ravelo, A.C., 2010. Palaeoclimate: Warmth and glaciation. Nature Geoscience 3: 672–674.
899 DOI:10.1038/ngeo965

900 Raymo, M.E., 1994. The initiation of Northern Hemisphere glaciation. Annual Review of
901 Earth and Planetary Sciences 22, 353-383.
902 http://dx.doi.org/10.1146/annurev.ea.22.050194.002033.

903 Raymo, M.E., Ruddiman, W.F., Backman, J., Clement, B. M., and Martinson, D.G., 1989.
904 Late Pliocene variation in Northern Hemisphere ice sheets and North Atlantic Deep Water
905 circulation. Paleoceanography 4: 413–446. DOI: 10.1029/PA004i004p00413.

906 Raymo, M. E., Lisiecki, L. & Nisancioglu, K.. 2006. Plio–Pleistocene ice volume, Antarctic
907 climate, and the global $\delta^{18}O$ record. Science 313: 492–495. DOI: 10.1126/science.1123296.

908 Reichart, G.J., Brinkhuis, H., 2003. Late Quaternary *Protoperidinium* cysts as indicators of
909 paleoproductivity in the northern Arabian Sea. Marine Micropaleontology 49 : 303-315.
910 https://doi.org/10.1016/S0377-8398(03)00050-1.

911 Rieley, G., Collier, R.J., Jones, D.M., Eglinton, G., 1991. The biogeochemistry of Ellesmere
912 Lake, U.K. I: source correlation of leaf wax inputs to the sedimentary lipid record. Organic
913 Geochemistry 17: 901–912. https://doi.org/10.1016/0146-6380(91)90031-E.

914 Rochon, A., de Vernal, A., Turon, J.L., Mathiessen, J., Head, M.J., 1999. Distribution of
915 recent dinoflagellate cysts in surface sediments from the North Atlantic Ocean and adjacent
916 seas in relation to sea-surface parameters: American Association of Stratigraphic
917 Palynologists Foundation Contributions Series 35, 150 pp.

Rosoff, D.B., and Corliss, B.H., 1992. An analysis of Recent deep-sea benthic foraminiferal morphotypes from the Norwegian and Greenland seas. Palaeogeography, Palaeoclimatology, Palaeoecology 91, 13-20. https://doi.org/10.1016/0031-0182(92)90028-4.

Ruddiman, W.F., Raymo, M., McIntyre, A., 1986. Matuyama 41,000-year cycles: North Atlantic Ocean and northern hemisphere ice sheets: Earth and Planetary Science Letters 80: 117-129. https://doi.org/10.1016/0012-821X(86)90024-5.

Sangiorgi, F. and Donders, T.H., 2004. Reconstructing 150 years of eutrophication in the north-western Adriatic Sea (Italy) using dinoflagellate cysts, pollen and spores. Estuarine, Coastal and Shelf Science 60: 69-79. https://doi.org/10.1016/j.ecss.2003.12.001.

Sangiorgi, F., Fabbri, D., Comandini, M., Gabbianelli, G. & Tagliavini, E., 2005. The distribution of sterols and organic-walled dinoflagellate cysts in surface sediments of the North-western Adriatic Sea (Italy). Estuarine, Coastal and Shelf Science 64: 395-406.

Shakun, J.D., Raymo, M.E., Lea, D.W., 2016. An early Pleistocene Mg/Ca-$\delta^{18}O$ record from the Gulf of Mexico: Evaluating ice sheet size and pacing in the 41-kyr world. Paleoceanography 31: 1011-1027. DOI: 10.1002/2016PA002956.

Seki, O., Foster, G.L., Schmidt, D.N., Mackensen, A., Kawamura, K., Pancost, R.D., 2010. Alkenone and boron-based Pliocene pCO_2 records. Earth and Planetary Science Letters 292: 201-211. http://dx.doi.org/10.1016/j.epsl.2010.01.037.

Shackleton, N.J. and Hall, M.A., 1984. Oxygen and carbon isotope stratigraphy of Deep Sea Drilling Project Hole 552A: Plio- Pleistocene glacial history. D-G. Roberts. D. Schnitker et al. initial Reports of the Deep Sea Drilling Project 81: 599-609. U.S. Govt. Printing Office, Washington.

Schreck, M., Meheust, M., Stein, R. and Matthiessen, J., 2013. Response of marine palynomorphs to Neogene climate cooling in the Iceland Sea (ODP Hole 907A). Marine Micropaleontology 101: 49-67. https://doi.org/10.1016/j.marmicro.2013.03.003.

Sinninghe Damsté, J.S., Schouten, S., Hopmans, E.C., van Duin, A.C.T., Geenevasen, J.A.J., 2002. Crenarchaeol: the characteristic core glycerol dibiphytanyl glycerol tetraether membrane lipid of cosmopolitan pelagic crenarchaeota. Journal of Lipid Research 43: 1641-1651. doi: 10.1194/jlr.M200148-JLR200

Sinninghe Damsté, J.S., 2016. Spatial heterogeneity of sources of branched tetraethers in shelf systems - The geochemistry of tetraethers in the Berau River delta (Kalimantan, Indonesia). Geochimica et Cosmochimica Acta 186: 13-31. https://doi.org/10.1016/j.gca.2016.04.033.

Sluijs, A., Pross, J., and Brinkhuis, H., 2005. From greenhouse to icehouse; organic-walled dinoflagellate cysts as paleoenvironmental indicators in the Paleogene. Earth Science Reviews 68: 281-315. https://doi.org/10.1016/j.earscirev.2004.06.001.

Sørensen, J. C., Gregersen, U., Breiner, M. and O. Michelsen, 1997. High-frequency sequence stratigraphy of Upper Cenozoic deposits in the central and southeastern North Sea areas.

955 Marine and Petroleum Geology 14 (2): 99-123. https://doi.org/10.1016/S0264-
956 8172(96)00052-9

957 Sosdian, S. Rosenthal, Y., 2009. Deep-sea temperature and ice volume changes across the
958 Pliocene-Pleistocene climate transitions. Science 325: 306-310.
959 DOI:10.1126/science.1169938 pmid:19608915.

960 Tabor, C.R., Poulsen, C.J., Pollard, D., 2014. Mending Milankovitch's theory: obliquity
961 amplification by surface feedbacks. Climate of the Past 10: 41–50. DOI: 10.5194/cp-10-41-
962 2014.

963 Thöle, H., Gaedicke, C., Kuhlmann, G., and Reinhardt, L., 2014. Late Cenozoic sedimentary
964 evolution of the German North Sea – A seismic stratigraphic approach. Newsletters on
965 Stratigraphy 47: 299–329. DOI: 10.1127/0078-0421/2014/0049.

966 Tzedakis, P.C., Crucifix, M., Mitsui, T., Wolff, E.W, 2017. A simple rule to determine which
967 insolation cycles lead to interglacials. Nature 542: 427–432 DOI:10.1038/nature21364.

968 Svenning, J.-C., 2003. Deterministic Plio-Pleistocene extinctions in the European cool-
969 temperate tree flora. Ecology Letters 6: 646–653. DOI: 10.1046/j.1461-0248.2003.00477.x.

970 Westerhoff, W., Donders, T.H. & Luthi, S.M., 2016. Report on ICDP workshop CONOSC
971 (COring the NOrth Sea Cenozoic). Scientific Drilling 21: 47-51. https://doi.org/10.5194/sd-
972 21-47-2016.

973 Whitehead, D.R., (1983). Wind pollination: some ecological and evolutionary perspectives.
974 In: Real, L. (Ed.), Pollination Biology. Academic Press, Orlando, pp.

975 Williams, G.L., Fensome, R.A., and MacRae, R.A., 2017. The Lentin and Williams index of
976 fossil dinoflagellates 2004 edition. American Association of Stratigraphic Palynologists,
977 Contributions Series 48, College Station, TX, 1097 pp. 97–108

978 Van der Vlerk, I.M, Florschütz, F. 1953. The palaeontological base of the subdivision of the
979 Pleistocene in the Netherlands. Verhandelingen Koninklijke Nederlandse Akademie van
980 Wetenschappen, Afdeling Natuurkunde, 1e Reeks XX(2): 1–58.

981 Versteegh, G.J.M., Zonneveld, K.A.F., 1994. Determination of (palaeo-)ecological
982 preferences of dinoflagellates by applying detrended and canonical correspondence analysis
983 to late Pliocene dinoflagellate cyst assemblages of the south Italian Singa section. Review of
984 Palaeobotany and Palynology 84: 181–199. https://doi.org/10.1016/0034-6667(94)90050-7.

985 Vonk, J.E., Gustafsson, Ö, 2009. Calibrating n-alkane *Sphagnum* proxies in sub-Arctic
986 Scandinavia. Organic Geochemistry 40: 1085-1090.
987 https://doi.org/10.1016/j.orggeochem.2009.07.002.

988 Zagwijn, W.H., 1960. Aspects of the Pliocene and early Pleistocene vegetation in The
989 Netherlands. Mededelingen van de Geologische Stichting, Serie C III-1–5, 1–78.

Zell, C., Kim, J.-H., Moreira-Turcq, P., Abril, G., Hopmans, E.C., Bonnet, M.-P., Sobrinho, R. L., and Sinninghe Damsté, J.S., 2013. Disentangling the origins of branched tetraether lipids and crenarchaeol in the lower Amazon River: implications for GDGT-based proxies, Limnology and Oceanography. 58, 343–353. DOI: 10.4319/lo.2013.58.1.0343.

Zhang, Z.-S., Nisancioglu, K. H., Chandler, M. A., Haywood, A. M., Otto-Bliesner, B. L., Ramstein, G., Stepanek, C., Abe-Ouchi, A., Chan, W.-L., Bragg, F. J., Contoux, C., Dolan, A. M., Hill, D. J., Jost, A., Kamae, Y., Lohmann, G., Lunt, D. J., Rosenbloom, N. A., Sohl, L. E., and Ueda, H., 2013. Mid-pliocene Atlantic Meridional Overturning Circulation not unlike modern. Climate of the Past 9, 1495-1504.DOI :10.5194/cp-9-1495-2013

Ziegler, P.A., 1990. Geological Atlas of Western and Central Europe (2nd edition).Shell Internationale Petroleum Maatschappij B.V.; Geological Society Publishing House (Bath), 239 pp.

Zöllmer, V. and Irion, G., 1996. Tonminerale des Nordseeraumes ihr Verteilungsmuster in kreidezeitlichen bis pleistozänen Sedimentabfolgen und in den Oberflächensedimenten der heutigen Nordsee: Courier Forschungsinstitut Senckenberg, 190. Frankfurt am Mainz, 72 p.

Zonneveld, K.A.F., Marret, F., Versteegh, G.J.M., Bogus, K., Bonnet, S., Bouimetarhan, I., Crouch, E., de Vernal, A., Elshanawany, R., Edwards, L., Esper, O., Forke, S., Grøsfjeld, K., Henry, M., Holzwarth, U., Kielt, J.-F., Kim, S.-Y., Ladouceur, S., Ledu, D., Chen, L., Limoges, A., Londeix, L., Lu, S.-H., Mahmoud, M.S., Marino, G., Matsouka, K., Matthiessen, J., Mildenhal, D.C., Mudie, P., Neil, H.L., Pospelova, V., Qi, Y., Radi, T., Richerol, T., Rochon, A., Sangiorgi, F., Solignac, S., Turon, J.-L., Verleye, T., Wang, Y. & Young, M., 2013. Atlas of modern dinoflagellate cyst distribution based on 2405 data points. Review of Palaeobotany and Palynology 191: 1-197.
https://doi.org/10.1016/j.revpalbo.2012.08.003.

Supplementary figures and data descriptions

Supplementary Figure 1: sedimentary facies interpretation of high-resolution seismically mapped surfaces S4-6 (see Fig. 2 for stratigraphical position) in relation to the wells. Approximate ages of the mapped surfaces are 2.8 Ma (S4), 2.44 Ma (S5) and 2.34 Ma (S6).

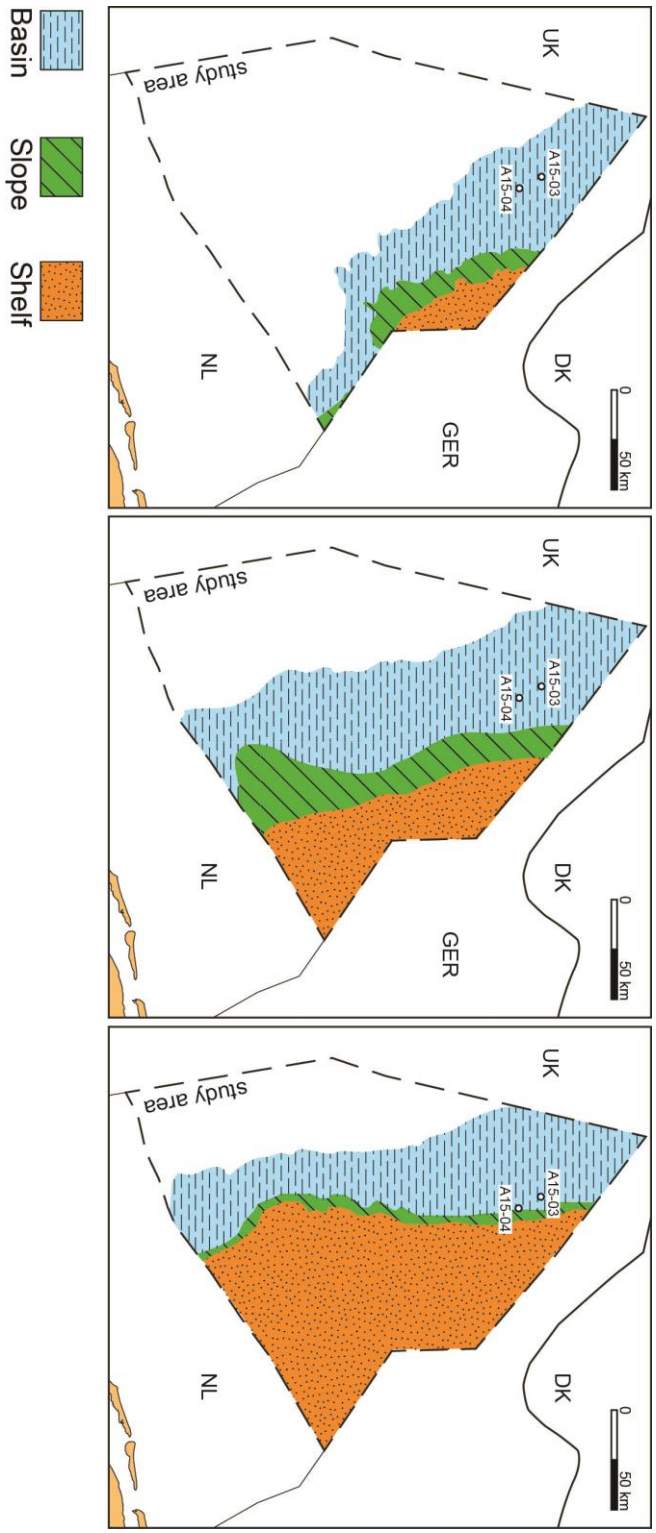

Supplementary Figure 2: Main pollen types in the spliced record of A15-3 (blue) and A15-4 (red) expressed as percentages of the total pollen. Dashed lines between AP % and T/M ratio indicate the observed lags of 3-8 kyr between (terrestrial) cooling and sea level decreases.

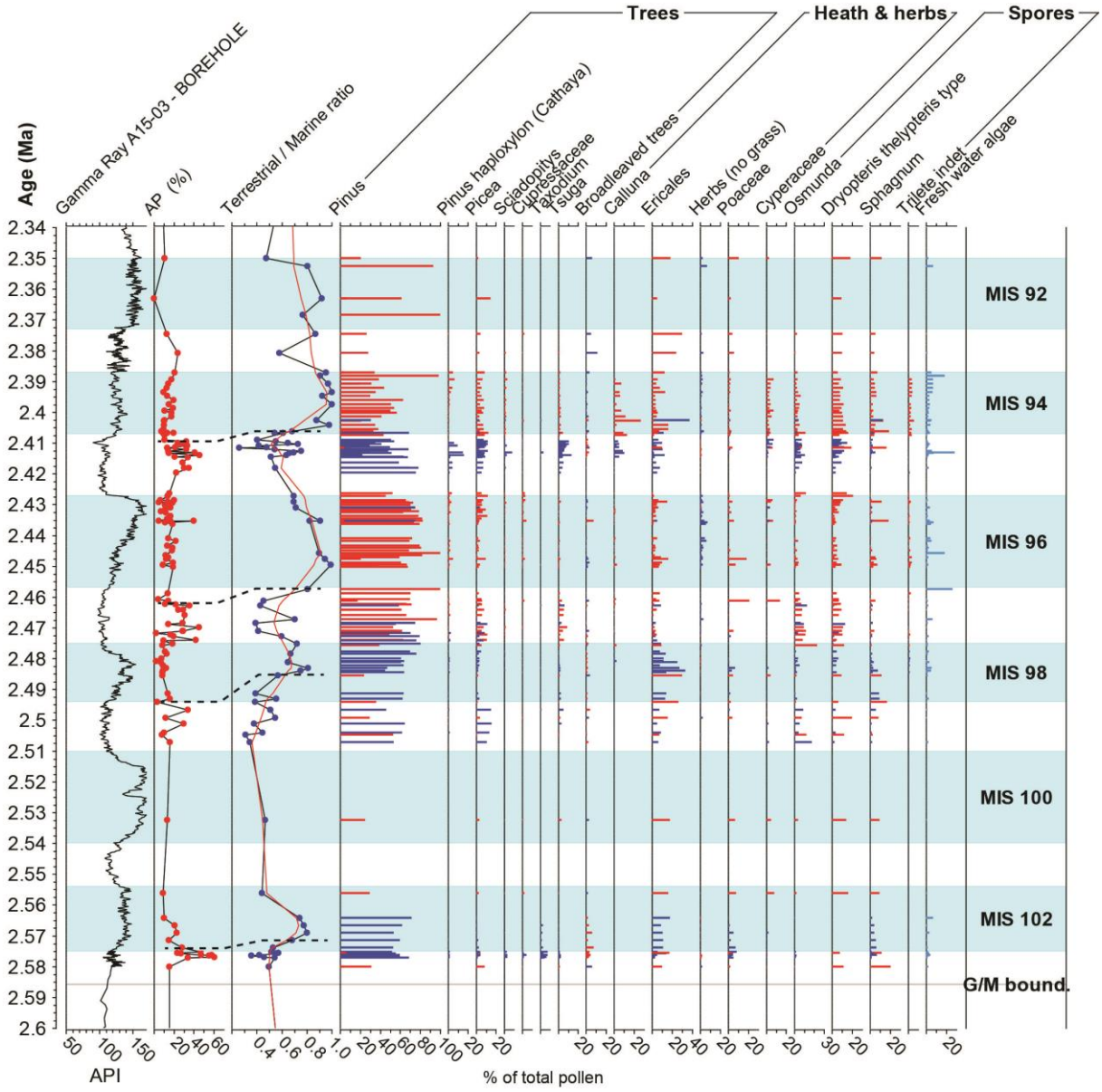

Supplementary Figure 3:

Age-depth model of the spliced A15-3 and A15-4 sections based on a smoothing spline interpolation (optimised range set to 1.65) of tie age points in Table S1 taken from Kuhlmann et al. (2006ab). The tie points where updated to recent range calibrations where necessary.

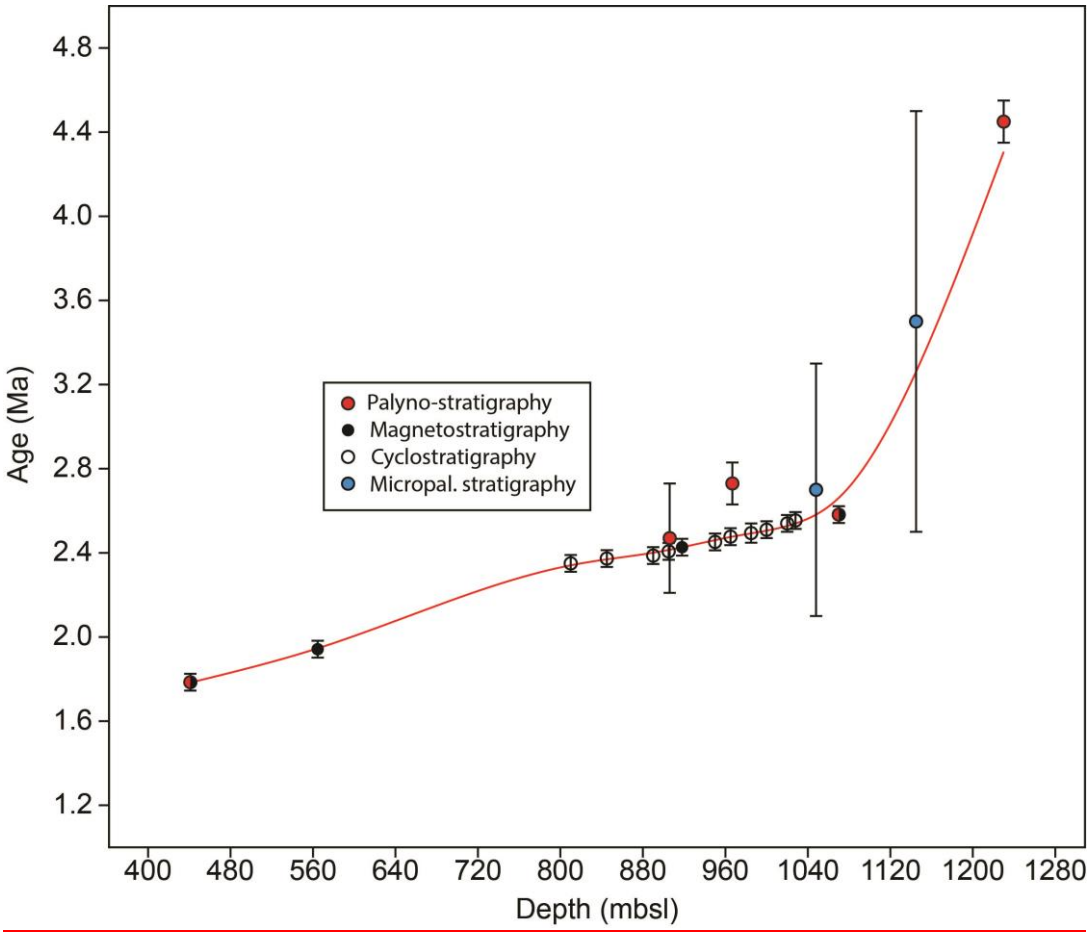

Supplementary Figure 4:

Well tie correlation points between A15-3 and A15-4 are based on the Gamma Ray correlation displayed in Fig. 2. The high R^2 of the linear relation between the well tie points confirms that the proxy records from both wells can by spliced confidently into a single record.

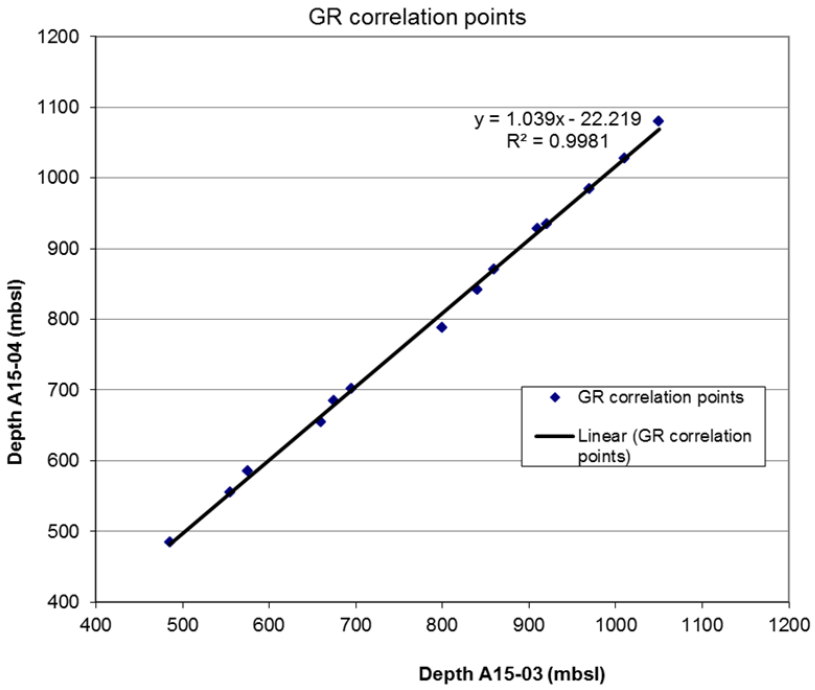

Supplementary Figure 5:

The terrestrial to marine palynomorph (T/M) ratio with in- and exclusion of bisaccate pollen show minimal offset, indicating a low influence of differential transport processes.

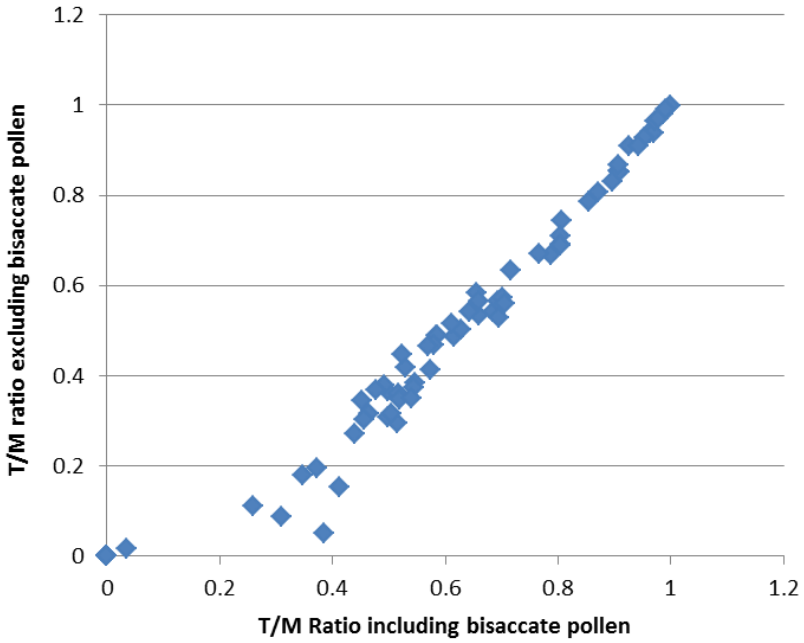

Supplementary Figure 6:

Ternary diagram based on the brGDGT analyses showing values close but not identical to the soil calibration. Samples with higher BIT (>0.5) show a greater correspondence to the soil calibration, which indicates some contribution of in-situ produced (aquatic) brGDGTs.

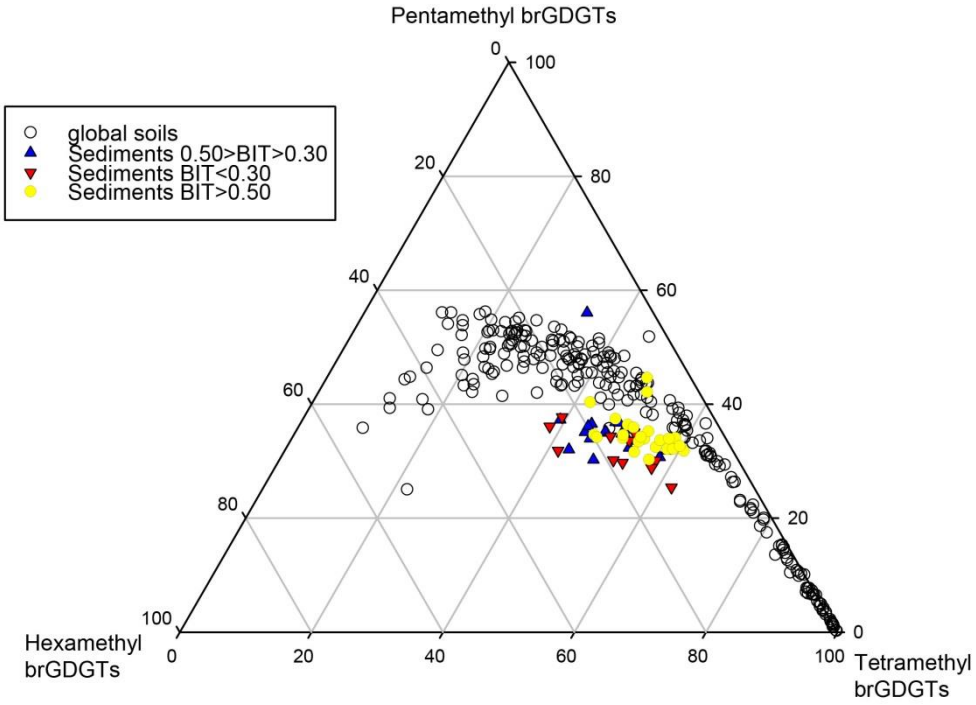

Supplementary Table S1

Chronostratigraphical control points taken from Kuhlmann et al. (2006ab). The tie points where updated to recent range calibrations where necessary. Minimum and maximum ages represent the range of ages from literature. Plotted ages represent the midpoints of these values. Miocene ages are not shown in Fig. S3 due to a hiatus at ~1240 mbsl separating the Miocene and Pliocene deposits (Kuhlmann et al., 2006ab).

Supplementary Table S2

Palynological abundance data of A15-3 and A15-4 by taxon and composite indices as displayed in Fig. 3. Percent data are based on a separate marine and terrestrial total.

Supplementary Table S3

Borehole Gamma Ray data (A15-3) and geochemical data of A15-3 and A15-4 (O and C stable isotope ratios, TOC, Alkane ratios, brGDGTs).